MS-No.: OS-2020-63

Title: Multidecadal Polynya Formation in a Conceptual (Box) Model

Author(s): Daan Boot, René M. van Westen and Henk A. Dijkstra

Point-by-point reply to reviewer #1

November 2, 2020

We thank David Bailey for his careful reading and for the useful comments on the manuscript.

Specific concerns:

1. *First off, it is extremely difficult to figure out exactly how these high resolution simulations were done. The authors refer to a manuscript in review (van Westen et al. 2020) for a description of the experiments. However, the model experiments and configuration are actually described in an earlier manuscript by van Westen and Dijkstra 2017. Please add more detail here about these simulations so the reader does not have to sift through the rest of the literature. Can the authors also comment about using year 2000 forcing as a control run for 250 years which is not a balanced climate?*

   Author's reply:
   In the revision we will include more information on the simulation of the Community Earth System Model (CESM). The results in van Westen and Dijkstra (2017) only cover the first 200 years of the simulation, while we use a period between model years 150 – 250. The complete CESM simulation (300 years) and full details can be found in van Westen et al. (2020) (https://doi.org/10.1038/s41598-020-71563-0).

   A present-day forcing (of the year 2000) is closer to current observations compared to pre-industrial control simulations (such as in CMIP). The author is right that the model is not in equilibrium, but the model has a spin-up period of 150 years. The upper ocean temperatures (1000 m) are fairly in equilibrium (see Figure S2 in van Westen et al. (2020)). Any drift can be removed by subtracting a linear or quadratic trend.

Note that pre-industrial control simulations of CMIP also are not in equilibrium, as the deep ocean fields take much longer time (millennial timescales) to equilibrate.

Changes in manuscript:
We will include a brief summary of the CESM simulation and equilibration and motivate the present-day configuration. For a complete overview of the full CESM results, we will refer to van Westen et al (2020).

2. *Here is my biggest concern. Based on the high resolution CESM simulations that I have seen (McClean et al. 2011; Kirtman et al. 2012; Small et al. 2014; Chang et al. (2020)) the mean state of the Antarctic sea ice is biased thin and not extensive enough. This I believe is one of the main reasons the polynyas do not show up in low resolution simulations, but do in the high resolution. That is, I believe that the polynyas are a result of a mean state bias. I realise this is more relevant to the van Westen et al. 2020 manuscript, but I think this should be addressed here as well. Also, this is a bit of semantic issue. Most of the polynyas that form in these high resolution simulations are sort of closed off embayments. As the ice grows in the SH, the Weddell gyre circulates sea ice to the East and eventually it meets up with the Maud Rise coastal area and encloses an open-ocean region. A polynya in my mind is when the area is completely sea ice covered in mid-winter and a hole opens up in the sea ice. Look at animations of daily sea ice concentration. The seasonality is the key here. At least stating the assumption that while polynya formation and the frequency of actual polynya events versus embayments in the CESM in these simulations may not be realistic, these are the processes behind this particular model simulation.*

Chang et al. (2020) Under review iHESP project paper.
Kirtman, B. P., et al. (2012), Impact of ocean model resolution on CCSM climate simulations, Clim. Dyn., 39, 1303â1328.
McClean, J., et al. (2011), A prototype two-decade fully-coupled fine-resolution CCSM simulation, Ocean Model., 39, 10â30.
Small, R. J., et al. (2014), A new synoptic scale resolving global climate simulation using the Community Earth System Model, J. Adv. Model. Earth Syst., 6, 1065â1094, doi:10.1002/2014MS000363.

Author's reply:
Thank you for the references. In van Westen and Dijkstra (2020a) they analyse a companion CESM simulation at a 1° resolution for 1300 years. One major difference between a low-resolution CESM (LR-CESM) and high-resolution CESM (HR-CESM) is the background stratification. The background stratification is much stronger in the LR-CESM, hence no deep convection developed over Maud Rise. This does not imply that no convection events occur in a low-resolution model. Dufour et al. (2017) demonstrate a different background stratification between a high- and low-resolution climate model which alters the periodicity of deep convection in the Weddell Sea.

Regarding the sea-ice thickness bias, van Westen and Dijkstra (2020b, https://os.copernicus.org/preprints/os-2020-33/) show the climatology of the sea-ice thickness over Maud Rise (their Figure 1d). The August sea-ice thickness is varying between 30 – 80 cm (90% range) with a time mean of about 53 cm for non-polynya years. Such values are also reported in an observation-model study in this part of the Weddell Sea (Holland et al. (2014), https://doi.org/10.1175/JCLI-D-13-00301.1). These daily-averaged (and also monthly-averaged) sea-ice fields clearly show that the polynya appears within the sea-ice and not by embayment as suggested by the reviewer.

Changes in manuscript:
We will discuss the results of the references provided by the reviewer regarding the potential biases. We will include an analysis of the daily-averaged sea-ice fields for model year 231 to show how these polynyas form in the CESM.

3. *The box model description is very confusing. Some of the terms in the equations are not described. While this might be in the Martinson et al. 1981 paper, some more detail should be repeated here. I guess the Martinson paper came up with the convention of h and H-h for the layer thicknesses. I would prefer h1 and h2 here. Similarly Regime I and III only have T, S, and rho instead of T1, S1, rho1, and T2, S2, and rho2. The Tb1, Sb1, and Tb2, Sb2 variables are introduced in the equations but not explained. I see these are mentioned later on in section 3.1. I think it is also very important to highlight what is different in the model description section from the Martinson et al. 1981 paper. Is it just that*

you used basically the same model, but with different forcing?

Author's reply:
The discussion of the equations was indeed quite minimal. The different terms in the equations will be discussed more elaborately. We will pay special attention to the sea-ice equation (following reviewer comment 2), and the horizontal advective fluxes related to T_{b1}, T_{b2}, S_{b1} and S_{b2}.

The convention of h, and $H - h$ is indeed from Martinson et al. (1981). The suggestion to change this to h_1 and h_2 for the two layers is followed with a depth H of the total layer.

The extensions to the Martinson model are: a dynamic subsurface layer, the horizontal advective fluxes, the forcing, and some parameter values have been changed. This issue is addressed in section 3.1. We will include this also in section 2.1.

Changes in manuscript:
The equations will be discussed more elaborately. The convention for the layer depths will be changed. The extensions/changes made with respect to the Martinson model will (also) be addressed in section 2.1.

Minor comments:

1. *What about Qio? I think this is more important when there is ice present in terms of forcing the ocean rather than Qia. Or does Qoa include Qio somehow? You have Qio from the CESM simulations already.*

   Author's reply:
   Q_{io} is modelled via a heat transfer flux given by the term: $\rho_0 \times C_p \times K(T - T_f)$ in equations 4a, 4c, 5a and 5c (as was done in Martinson et al., 1981). This means Q_{oa} does not include Q_{io}.

   Changes in manuscript:
   In the model description (2.1) the equations will be discussed more elaborately. There it will also be made clear that this term represents the heat flux between the sea ice and the ocean.

2. *Are there any other freshwater flux observations around Antarctica? Are these open ocean only or ice-ocean?*

   Author's reply:
   There are several observations, see for example in Trenberth et al. (2007) where they show evaporation minus precipitation in their Figure 3. The value seen there, corresponds to the value used in this paper. This is based on ERA-40 data. This includes reanalyzed data for open ocean and ice-ocean.

   Changes in manuscript:
   No changes necessary.

3. *I'm curious why you used fitted background T and S. You have the data from the CESM run, so why not use that?*

   Author's reply:
   We are using a highly idealized model and it is not suitable to reproduce the CESM simulation accurately. We believe the model is suitable to test high level hypotheses: a subsurface accumulation of heat is important for polynya formation, and a periodic subsurface accumulation of heat results in periodic polynya formation. It is more suitable to use an idealized subsurface heat and salt flux for the model than the noisy CESM data.

   Changes in manuscript:
   The above reasoning will be included in the revised text.

4. *Figure 4 is missing labels on the density contours and the salinity axis.*

   Author's reply:
   This was done purposefully to clearly show the different cycles in the T-S space. If we would have used the actual values for salinity and density, the plots would overlap, making the plot unclear (see for example Figure 9c which includes the three cycles also shown in Figure 4).

   We did include the temperature values since these are important for the onset of sea-ice growth. The salinity values are not that important for showing the general behavior. Since we do not use actual salinity values, we cannot compute the density with equation 1. Therefore, there are also no density values on the contour lines. We made sure

that the scale of the salinity axis is the same for each cycle, so they can be compared.

Changes in manuscript:
We will make changes in the caption and the main text to clarify this issue.

5. *Figure 5 (and others). Why did you plot thickness as a measure of polynya presence? The definition is concentration based. Panels b and e in Figure 5 are not that helpful. The thickness is the same every year. The shading indicates there is a constant polynya in panel e right? Where on the T-S curve is the active polynya. It should only be during Regime IV, i.e. while on the straight line between density 1027.8 and 1027.7? Actually, how can you say MKH is a polynya? It looks ice free the whole year? I'm very confused here.*

Author's reply:
The model does not determine sea-ice concentration. The sea-ice thickness is plotted in Figures 7-9 to show the difference between polynya and non-polynya periods. For consistency we also plotted the sea-ice thickness in Figure 5. Again for consistency, we included the shading. Furthermore, it also shows that the sea-ice thickness remains constant for these two cases (in Figure 5).

The polynya definition we are using for this model is shown on pg. 10 l. 15. Following this definition, we can say that MKH is basically one long polynya period, with polynya formation every year. Every year there is a little bit of ice formation (about 10 cm), and due to the brine rejection of this sea-ice formation, the water column becomes unstable, mixing warm waters to the surface and melting the sea-ice. Case MKH can be compared with the 2-overturn cycle in Figure 4. At point D (in Figure 4) the polynya has formed. This point is not clearly visible in Fig. 5f, but it is located around (T, S) = (0.6, 34.7), around the 'kink' between the two straight lines.

The results of case MKH are of course odd, but that is because we believe important physics are missing in this case. We do call it a polynya to be consistent with the other cases.

Changes in manuscript:
We will include a more extensive discussion of cases MKL and MKH where we will address the significance of Figures 5b and 5e, and why we do call it a polynya period.

6. *Figure 6. Can you indicate the actual polynya years in CESM here? Is it every year? Similarly for Figure 7.*

   Author's reply:
   The polynya years are addressed in the caption of Figure 6. The polynya years for Figures 7-9 are also clear from the shading in subfigures a and b.

   Changes in manuscript:
   The color codes corresponding to polynya years will be added in the captions for Figures 6-9.

7. *In the summary and discussion, the authors mention that this box model is slightly extended. This needs to be expanded. You could not replicate the results from Martinson as I understand it. More detail here on what is new about your study!*

   Author's reply:
   The main extension of the model is the inclusion of subsurface advection of heat and salt for both layers. Although we couldn't exactly replicate results from Martinson, we considered a case in which there is no subsurface advection (e.g. reference case). This set-up was the original set-up of Martinson and we found similar (not identical) results as reported in Martinson et al. (1981). All the other experiments have subsurface advection in the layers.

   Changes in manuscript:
   We will discuss and highlight the extensions of the original Martinson model in the discussion.

8. *Also, I sort of feel like it is missing a big punchline. What have you added to the body of literature on Maud Rise polynyas here? Is it just the enhanced role of subsurface heat accumulation? The results from the van Westen work were not simulated with the box model, but I think more needs to be added here to explain what the box model gives you and adds to the story.*

Author's reply:
Our starting point is the Martinson paper. In our view, this paper has a large influence on the general paradigm on Maud Rise polynya formation (i.e. deep convection induced by surface processes). What we have shown is that this model is not capable of simulating multiple polynya events as is seen in observations (e.g. the 1970s, 1980, 1994, and the 2016-17 event). When this model is extended, with most prominently (periodic) subsurface heat and salt accumulation, the model is capable of simulating multiple events. This is an improvement of the original model, which also sheds another light on the processes responsible for polynya formation.

Our model is very simple and includes only a few basic physical processes compared to that of the high-resolution CESM. Nevertheless, our model is capable of qualitatively reproducing the CESM simulation. This suggests that the most important physical processes are included in our model. The results suggest that subsurface heat and salt accumulation play an important role in polynya formation. Processes which have not been discussed often in the 'polynya literature'. Most studies only investigate surface instabilities (e.g. brine rejection) rather than subsurface processes. Surface forcing, which is also incorporated in the box model, is random and not causing polynya formation. Surface related processes cannot completely explain polynya formation nor its periodicity (if such a multidecadal period exists in the Southern Ocean, see discussion van Westen and Dijkstra (2020a)).

Changes in manuscript:
An extra paragraph will be added to highlight these findings and that the subsurface related processes need to be investigated in future research of the Maud Rise polynya.

References:

– Holland et al. (2014), Modeled Trends in Antarctic Sea Ice Thickness, https://doi.org/10.1175/JCLI-D-13-00301.1

– Trenberth et al. (2007). Estimates of the global water budget and its annual cycle using observational and model data, https://doi.org/10.1175/JHM600.1

– van Westen et al. (2020), Ocean model resolution dependence of Caribbean sea-level projections, https://doi.org/10.1038/s41598-020-71563-0

– van Westen and Dijkstra (2020a), Multidecadal Preconditioning of the Maud Rise Polynya Region, https://doi.org/10.5194/os-2020-25

– van Westen and Dijkstra (2020b), Subsurface Initiation of Deep Convection near Maud Rise, https://doi.org/10.5194/os-2020-33

MS-No.: OS-2020-63

Title: Multidecadal Polynya Formation in a Conceptual (Box) Model

Author(s): Daan Boot, René M. van Westen and Henk A. Dijkstra

Point-by-point reply to reviewer #2

November 2, 2020

We thank Wilbert Weijer for his careful reading and for the useful comments on the manuscript.

1. *p.1, l. 12: Usually a distinction is made between MRPs, which are clearly related to bathymetry; and the larger Weddell Sea Polynyas (WSPs) which are not related to bathymetry, as exemplified by those observed in the mid-70s. I suggest that the authors note this distinction.*

   Author's reply:
   Thank you for the notification. We will address this issue in the introduction.

   Changes in manuscript:
   The distinction between MRPs and WSPs will be made in the introduction.

2. *p.3, l. 2: vertical -> vertically stacked.*
   Author's reply:
   Suggestion followed.

   Changes in manuscript:
   The text will be changed accordingly.

3. *p.3, l. 27: remove 'a'*

   Author's reply:
   Suggestion followed.

   Changes in manuscript:
   The text will be changed accordingly.

4. *p. 5-6: In my opinion, the model description is adequate, maybe with the exception of the sea ice equation, which could use some clarification.*

   Author's reply:
   We agree, we will clarify the sea-ice equation.

   Changes in manuscript:
   The equations, including the sea ice equation, will be discussed more elaborately.

5. *p. 9, Caption Table 2: What do the 'bars' refer to? Overbars?*

   Author's reply:
   Yes, they refer to overbars.

   Changes in manuscript:
   The caption will be changed accordingly.

6. *p. 9, l. 21: So are these fluxes averaged over the polynya region?*

   Author's reply:
   Yes, they are spatially averaged over the 'polynya region' identified in Van Westen and Dijkstra (2020) (2°E – 11°E × 63.5°S – 66.5°S). This is mentioned in Figure 2.

   Changes in manuscript:
   The spatially averaging will also be mentioned in the main text, and the caption of Table 3.

7. *p. 10, l. 7: It would probably be good to explicitly state that this is a prescribed 25-yr cycle.*

   Author's reply:
   Suggestion followed.

   Changes in manuscript:
   It will be explicitly stated in the text that the forcing in the box model has a prescribed 25-year period.

8. *p. 10, l. 9: I think it would be good to have a better justification of the advective terms somewhere. A source of heat or salt is of course a consequence of a /divergence/ of advective fluxes. Maybe a better paradigm is that the lower box is âbathingâ in a water mass with ambient temperature T_{b2} and salinity S_{b2}.*

Author's reply:
The reasoning behind the advective fluxes is that the layers do not drift away from the surrounding water masses. This reasoning follows your suggested paradigm. This has not been made explicit in the text. We will do that.

Changes in manuscript:
The justification of the advection terms will be changed to give a more physical point of view, as suggested in the above comment.

9. *p.10, l. 16: I suspect you mean ocean cooling, so heat transfer from the ocean to atmosphere. This would mean warming of the atmosphere.*

   Author's reply:
   Yes, that is what is meant here.

   Changes in manuscript:
   The statement in the text will be clarified.

10. *p. 11, Fig. 3: I'm a bit concerned by the strong variations, especially in the later years. I assume that the authors have checked that this water mass was not influenced by a polynya in the CESM? Evidently, you want to force the box model with upstream conditions.*

    Author's reply:
    We agree that forcing the model should be forced with upstream data. We therefore used a different region for fitting the subsurface fluxes (11°E – 12°E × 63.5°S – 66.5°S). We performed the model simulations with the new subsurface fluxes. The results become more convincing with the new fluxes. Especially case PFB improves with respect to the CESM simulation. Also the 25-year period becomes more apparent in the spectral analysis.

    Changes in manuscript:
    The new subsurface fluxes will be added, as well as the new results and a new discussion on the results.

11. *p. 15, l. 25-29: Maybe you can leave out the inclusion of the factor 35 (or discuss it somewhere else)? As it stands, F_N is /not/ a freshwater flux, as claimed in l. 27, but a salt flux. Besides, it would result in a sign error.*

Author's reply:
Suggestion followed.

Changes in manuscript:
The text will be changed accordingly.

12. *p. 20-21: I think we are missing some rules for T_2 and S_2 in certain transitions.*

Author's reply:
You are right, those are missing.

Changes in manuscript:
The missing information will be included in the revision.

13. *In our recent paper (Kaufman et al. 2020) we studied the heat content in E3SMv0-HR (a close clone of CESM1), and also found that heat build-up preceded polynya formation. However, our analysis suggests that this heat build-up is driven by a reduced surface heat loss under ice-covered conditions, and not an enhanced ocean heat import (Fig. 8c). In fact, ocean heat advection appeared to counteract the heat accumulation by removing excess heat. I suppose that in the context of this box model, this situation would be represented by $T_2 > T_{b2}$ for long periods of time without polynyas. Does a situation like this occur in your model, and can you discuss the context of these occurrences?*

Reference: Kaufman, Z.S., Feldl, N., Weijer, W. and Veneziani, M., 2020. Causal Interactions between Southern Ocean Polynyas and High-Latitude Atmosphere Ocean Variability. Journal of Climate, 33(11), pp.4891-4905.

Author's reply:
In our box model the situation that $T_2 > T_{b2}$ does not occur. The advective flux is thus always a source of heat to the subsurface layer. T_2 is always smaller than T_{b2} because the subsurface layer loses heat to the surface layer via the term $K_T(T_1 - T_2)$.

Changes in manuscript:
This will be discussed in the revised manuscript.

References:

– van Westen and Dijkstra (2020), Multidecadal Preconditioning of the Maud Rise Polynya Region, https://doi.org/10.5194/os-2020-25

List of all relevant changes:

- The subsurface fluxes have been fitted to a different region. This means we have used different subsurface fluxes. The description, figures and discussion have been revised. The results have not changed qualitatively and have become more convincing. The data sets made available have also been updated.
- In Section 2 a paragraph has been added regarding the CESM simulation used for this study. Polynya formation in the simulation is also addressed in this paragraph.
- The discussion of the model equations is more elaborate.
- Section 4 (Summary and discussion) is extended with an extra paragraph highlighting our findings.
- The convention h, and H-h for the layer dephts has been changed to h_1 and h_2.
- Other changes are relatively minor and mostly small textual changes.

Multidecadal Polynya Formation in a Conceptual (Box) Model

Daan Boot[1], René M. van Westen[1], and Henk A. Dijkstra[1,2]

[1]Institute for Marine and Atmospheric research Utrecht, Department of Physics, Utrecht University, Utrecht, the Netherlands
[2]Center for Complex Systems Studies, Utrecht University, Utrecht, the Netherlands

Correspondence to: D. Boot <d.boot@uu.nl>

Abstract. Maud Rise Polynyas (MRPs) form due to deep convection, which is caused by static instability of the water column. Recent studies with the Community Earth System Model (CESM) have indicated that a multidecadal varying heat accumulation in the subsurface layer occurs prior to MRP formation due to the heat transport over the Weddell gyre. In this study, a conceptual MRP box model, forced with CESM data, is used to investigate the role of this subsurface heat accumulation in MRP formation. Cases excluding and including multidecadal varying subsurface heat and salt fluxes are considered and multiple polynya events are only simulated in the cases where subsurface fluxes are included. The dominant frequency for MRP events in these results, approximately the frequency of the subsurface heat and salt accumulation, is still visible in cases where white noise is added to the freshwater flux. This indicates the importance and dominance of the subsurface heat accumulation in MRP formation.

1 Introduction

~~A Maud Rise Polynya (MRP), a large hole in the Antarctic sea-ice pack,~~ The Weddell Sea is a region where open-ocean polynyas occassionaly form. A distinction is made between the larger Weddell Sea Polynyas (WSPs), and the smaller scaled Maud Rise Polynyas (MRPs). Formation of the latter is clearly related to bathymetry, i.e. Maud Rise, an underwater seamount, while this clear relation is absent for the former. Such an MRP appeared again in 2016 and 2017 (Jena et al., 2019). The first ~~MRPs~~ polynyas in the Weddell Sea were observed in the 1970s around 65°S and 0°E (Martinson et al., 1981) with in-situ observations (Gordon, 1978) and first available satellite images (Carsey, 1980). In 1974, 1975, and 1976 polynyas with an areal extent of approximately 2.5×10^5 km^2 were present during the entire winter (Gordon et al., 2007), and can be classified as WSPs. The 2017 MRP had an approximate area of 0.5×10^5 km^2 and persisted from September to October (Campbell et al., 2019; Cheon and Gordon, 2019). Observations also suggest a short-lived and small-scaled MRP in 1994 (Holland, 2001; Lindsay et al., 2004). In this paper we will focus specifically on MRPs.

Many studies have looked into the processes responsible for MRP formation. A key theory is that the MRP is formed by deep convection caused by static instability due to surface salt anomalies in a preconditioned water column (Martinson et al., 1981). Such salt anomalies can be caused by brine rejection (Martinson et al., 1981) but also by freshwater flux anomalies due to variations in the Southern Annular Mode (Gordon et al., 2007; Cheon and Gordon, 2019). Another line of work focuses on dynamical forcing by the wind (Parkinson, 1983; Francis et al., 2019; Jena et al., 2019; Campbell et al., 2019) as a cause of MRP formation. A divergent wind stress can open up the sea-ice pack and induce upwelling (by Ekman dynamics) which either causes an MRP directly or induces deep convection. Finally, dynamical forcing through ocean eddy shedding at the flanks of

Maud Rise (Holland, 2001) and Taylor caps above Maud Rise (Alverson and Owens, 1996; Kurtakoti et al., 2018) can change the background stratification and hence precondition the water column. These processes also cause a general halo of relatively low sea-ice concentrations over Maud Rise (Lindsay et al., 2004).

Climate models provide the opportunity to study deep convection and consequently MRP formation. From several climate models, it is known that deep convection in the Southern Ocean varies on multidecadal to multicentennial time scales (Martin et al., 2013; Zanowski et al., 2015; Latif et al., 2017; Weijer et al., 2017). Several climate models show subsurface heat accumulation prior to deep convection, e.g. in the Kiel Climate Model (KCM) (Martin et al., 2013), the Community Earth System Model (CESM) (van Westen and Dijkstra, 2020a) and the Geophysical Fluid Dynamics Laboratory Climate Model (GFDL CM2-0) (Dufour et al., 2017). Through buoyancy gain in the subsurface layer, deep convection is induced, which results in MRP formation (Martin et al., 2013; Latif et al., 2017; Reintges et al., 2017). In the KCM, for example, a stronger stratification results in a longer period for deep convection, because more buoyancy gain is necessary to overcome the more stable stratification (Latif et al., 2017; Reintges et al., 2017). Another important feature is model resolution as shown by Weijer et al. (2017): MRPs were found in a high-resolution (0.1°) version of the CESM, whereas in the low-resolution (1°) version of the same model no MRPs were simulated. Dufour et al. (2017) used the GFDL CM2-0 model with a nominal ocean grid spacing of 0.25° and 0.1° and they show that the occurrence of deep convection itself is not sufficient to create MRPs. If the subsurface heat reservoir cannot supply enough heat to melt all the sea ice, an MRP will not form.

A recent model study by van Westen and Dijkstra (2020a) shows a multidecadal occurrence of MRPs and suggest that the time scale of MRP formation is affected by intrinsic ocean variability through subsurface preconditioning. They relate the subsurface heat accumulation near Maud Rise to the Southern Ocean Mode (SOM), a multidecadal mode of intrinsic variability in the Southern Ocean caused by eddy-mean flow interactions (Le Bars et al., 2016; Jüling et al., 2018), which is present in high-resolution (ocean) models (van Westen and Dijkstra, 2017). van Westen and Dijkstra (2020a) show that heat content anomalies propagate from the SOM region (50°S – 35°S $\times$ 50°W – 0°W) via the Antarctic Circumpolar Current (ACC) to 30°E, and the Weddell Gyre to the Maud Rise area where they cause heat accumulation in the subsurface layer. The CESM model results are further analysed in van Westen and Dijkstra (2020b) where the importance of this subsurface heat accumulation on the MRP formation is shown.

To better understand the results of the high-resolution CESM simulations (van Westen and Dijkstra, 2020a, b), and to connect to earlier theories of MRP formation, we use here an extension of the Martinson et al. (1981) box model. The original model is extended with a dynamical subsurface layer and (advective) heat and salt fluxes are added as a forcing to the subsurface layer. This extended version of the Martinson model is described in Section 2. Results for five different cases are considered (Section 3), to address the importance of subsurface forcing (i.e. heat and salt accumulation) relative to surface forcing (e.g., brine rejection, wind forcing) in MRP formation, and the processes determining the long-term variability of MRPs. In Section 4 a summary and discussion of the results is given.

2 Model description and cases considered

The model ~~below~~ used is a slightly extended version of the box model used in Martinson et al. (1981). The ~~extended~~ Martinson model is extended with horizontal advective salt and heat fluxes and a dynamic subsurface layer. Furthermore, we have used a different forcing and different parameter values. The extended model is described (Section 2.1), the CESM simulation used in this study is discussed in Section 2.2 and the different configurations and cases are discussed in Section ~~2.2~~2.3.

2.1 Model Description

The MRP box model consists of two ~~vertical~~ vertically stacked boxes with a constant depth and within each box the ocean properties (e.g. temperature and salinity) are uniform. The model simulates the development of temperature (T), salinity (S), and sea-ice thickness (δ) in each box under surface and subsurface forcing. The depth of the entire water column is H with the surface layer having a depth ~~h~~ of h_1 and the subsurface layer a depth ~~$H - h$~~of h_2.

The model has four different flow regimes, below referred to as regimes, which are differentiated on sea-ice cover (sea-ice free versus sea-ice covered) and static stability (two layered versus mixed). Whenever stable/unstable is mentioned below, we refer to static stability of the water column, so no dynamical instabilities. There are the sea-ice free regimes I and II, and the sea-ice covered regimes III and IV. Regimes II and IV are stably stratified ($\rho_1 < \rho_2$), and regimes I and III are mixed with one uniform density over the entire depth (Fig. 1). The subscripts 1 and 2 correspond to the surface and subsurface layer, respectively.

Over time the model state may transit through these four regimes under the influence of (seasonal) forcing. The four different regime transitions are indicated by the arrows in Fig. 1, i.e.,

(a) From sea-ice covered regimes to sea-ice free regimes due to complete melt of the sea ice ($\delta = 0$) (regime IV $\rightarrow$ II or regime III $\rightarrow$ I). Temperature and salinity are uniform over the entire layer and given by T and S instead of T_n and S_n where n is either 1 or 2,

(b) from sea-ice free regimes to sea-ice covered regimes, because the surface layer reaches freezing temperature and sea ice starts to form ($T_1 = T_f$) (regime II $\rightarrow$ IV, and regime I $\rightarrow$ III),

(c) from stable, two layered regimes to unstable, mixed regimes, because the density of the surface layer is equal to or larger than that of the subsurface layer ($\rho_1 \geq \rho_2$) (regime II $\rightarrow$ I, and regime IV $\rightarrow$ III). The water column becomes unstable and mixes through overturning. Temperature and salinity are uniform over the entire layer and given by T and S instead of T_n and S_n, and

(d) from unstable, mixed regimes to stable, two layered regimes, because of stabilisation of the water column due to a decreasing density of the mixed layer (regime I $\rightarrow$ II, and regime III $\rightarrow$ IV).

The precise conditions for the regime transitions are shown in Appendix A. It should be noted that for the model to switch between regimes I (mixed, sea-ice free) and III (mixed, sea-ice covered) the entire water column should reach freezing temperature, which is physically not realistic. Therefore, this transition does not exist in the model (regime I $\nrightarrow$ regime III)

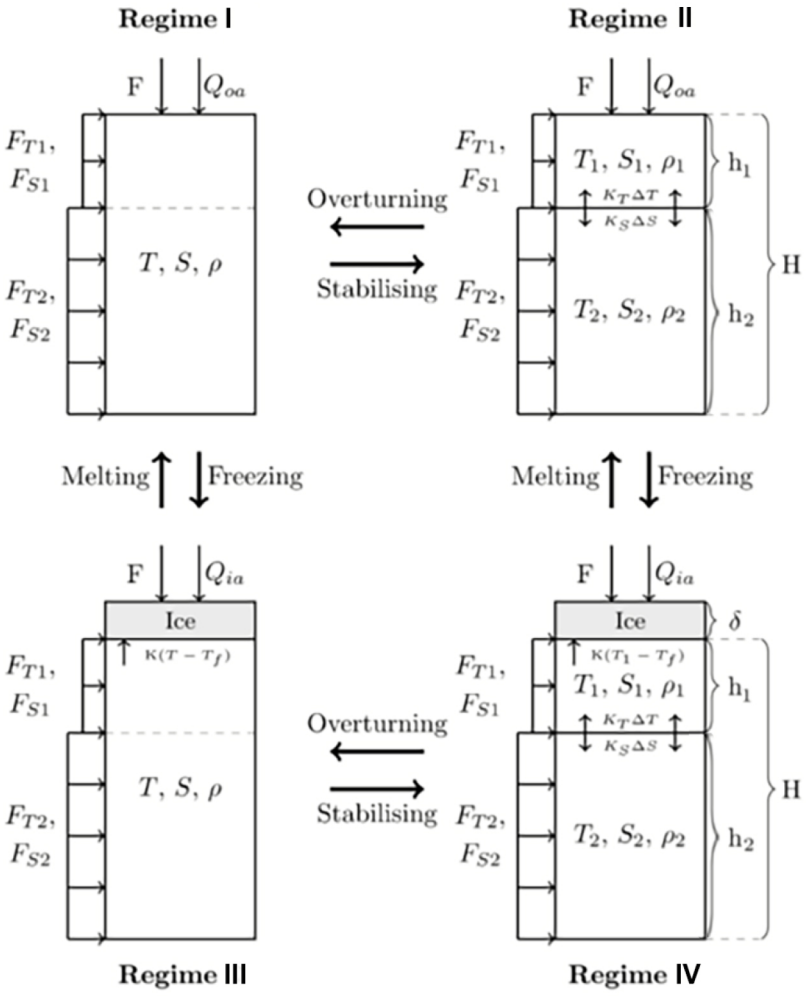

Figure 1. A schematic representation of the different regimes of the extension of the model used in Martinson et al. (1981). The parameters displayed in the figure are explained in the text. The directions and size of the arrows are not necessarily a representation of the actual direction and magnitude of the fluxes. The actual size and direction are dependent on the state of the model. Positive fluxes represent fluxes entering the water column. Regime transitions are shown by bold arrows.

The model is forced at the surface by a freshwater flux F, and by a heat flux Q_{ia} for sea-ice covered regimes and Q_{oa} for open-ocean regimes. Both the surface and subsurface layer are subject to ~~a~~ horizontal advective heat and salt fluxes (F_{T1} and F_{S1} for the surface layer, and F_{T2} and F_{S2} for the subsurface layer) which depend on a background value (T_{b1} and S_{b1} for the surface layer, and T_{b2} and S_{b2} for the subsurface layer) and a relaxation timescale (τ).

The heat and salt transfer between the layers are modelled using exchange coefficients (K_T and K_S), which account for upwelling, turbulent exchange and diffusion. In sea-ice covered regimes there is a heat flux present between the sea ice and the

underlying layer. This heat flux is modelled using a turbulent exchange coefficient (K). Brine is rejected during sea-ice growth and freshwater is added to the surface layer during sea-ice melt, brine rejection and sea-ice melt are modelled using a constant representing the salinity difference between sea ice and seawater (σ) and the rate of sea-ice growth ($d\delta/dt$). The density for each layer is determined from a simple linear equation of state:

$$\rho = \rho_0(1 - \alpha T + \beta S) \tag{1}$$

where the constants α and β are the thermal expansion and haline contraction coefficients, respectively.

The governing equations for each regime are then:

Regime I:

$$H\frac{dT}{dt} = \frac{Q_{oa}}{\rho_0 C_p} + \tau(T_{b1} - T)h_1 + \tau(T_{b2} - T)(H - h)h_2 \tag{2a}$$

$$H\frac{dS}{dt} = -F + \tau(S_{b1} - S)h_1 + \tau(S_{b2} - S)(H - h)h_2 \tag{2b}$$

$$\delta = 0 \tag{2c}$$

Regime II:

$$h_1\frac{dT_1}{dt} = \frac{Q_{oa}}{\rho_0 C_p} + K_T(T_2 - T_1) + \tau(T_{b1} - T_1)h_1 \tag{3a}$$

$$h_1\frac{dS_1}{dt} = K_S(S_2 - S_1) - F + \tau(S_{b1} - S_1)h_1 \tag{3b}$$

$$\delta = 0 \tag{3c}$$

$$\frac{dT_2}{dt} = \tau(T_{b2} - T_2) + \frac{K_T(T_1 - T_2)}{H - h}\frac{K_T(T_1 - T_2)}{h_2} \tag{3d}$$

$$\frac{dS_2}{dt} = \tau(S_{b2} - S_2) + \frac{K_S(S_1 - S_2)}{H - h}\frac{K_S(S_1 - S_2)}{h_2} \tag{3e}$$

Regime III:

$$H\frac{dT}{dt} = K(T - T_f) + \tau(T_{b1} - T)h_1 + \tau(T_{b2} - T)(H - h)h_2 \tag{4a}$$

$$H\frac{dS}{dt} = \sigma\frac{d\delta}{dt} - F + \tau(S_{b1} - S)h + \tau(S_{b2} - S)(H - h)h_2 \tag{4b}$$

$$\frac{d\delta}{dt} = \frac{1}{\rho_i L}(-Q_{ia} - \rho_0 C_p K(T - T_f)) + \frac{F}{\sigma} \tag{4c}$$

Regime IV:

$$h_1 \frac{dT_1}{dt} = K_T(T_2 - T_1) - K(T_1 - T_f) + \tau(T_{b1} - T_1)h_1 \tag{5a}$$

$$h_1 \frac{dS_1}{dt} = \sigma \frac{d\delta}{dt} - F + \tau(S_{b1} - S_1)h_1 \tag{5b}$$

$$\frac{d\delta}{dt} = \frac{1}{\rho_i L}(-Q_{ia} - \rho_0 C_p K(T_1 - T_f)) + \frac{F}{\sigma} \tag{5c}$$

$$\frac{dT_2}{dt} = \tau(T_{b2} - T_2) + \frac{K_T(T_1 - T_2)}{H - h}\,\frac{K_T(T_1 - T_2)}{h_2} \tag{5d}$$

$$\frac{dS_2}{dt} = \tau(S_{b2} - S_2) + \frac{K_S(S_1 - S_2)}{H - h}\,\frac{K_S(S_1 - S_2)}{h_2} \tag{5e}$$

In these equations, C_p is the specific heat of seawater with a reference density ρ_0. Sea ice has a density of ρ_i and a latent heat of melting/freezing indicated by L. The standard values of all parameters used in the model are presented in Section ~~2.2~~ 2.3 below.

In the temperature equations the ocean-atmosphere and ice-ocean heat flux, horizontal advective fluxes, and heat transfer between the two layers are represented.. The ocean-atmosphere flux is given by $Q_{oa}\rho_0 C_p h_n$, where h_n is either H (regimes I and III) or h_1 (regimes II and IV). The horizontal advective fluxes are given by $\tau(T_{b1} - T_n)$ (surface) and $\tau(T_{b2} - T_n)$ (subsurface), where T_n is either T (regimes I and III), T_1 (surface flux, regimes II and IV) or T_2 (subsurface flux, regimes II and IV). The heat transfer between the sea-ice and the surface layer is given by $\frac{K(T_n - T_f)}{h_n}$ where T_n is either T or T_1, and $h_n$is either h_1 or H depending whether the model is in regime III or regime IV. Lastly, the heat transfer between the layers in regimes II and IV are given by $\frac{K_T(T_n - T_m)}{h_n}$ where n and m are either 1 or 2.

In the salinity equations the freshwater flux, sea ice melt and brine rejection, horizontal advective fluxes and salt transfer between the two layers are represented. The freshwater flux is given by $\frac{F}{h_n}$, where h_n is either H or h_1. The horizontal advective fluxes are given by $\tau(S_{b1} - S_n)$ (surface) and $\tau(S_{b2} - S_n)$ (subsurface), where S_n is either S (regime I and III), S_1 (surface flux, regimes II and IV) or S_2 (subsurface flux, regimes II and IV). The salt transfer between the layers in regimes II and IV is given by $\frac{K_S(S_n - S_m)}{h_n}$ where n and m are either 1 or 2. Brine rejection and sea ice melt are given by $\sigma\frac{d\delta}{dt}$.

The sea-ice thickness is dependent on heat transfer between the sea ice and the ocean and the atmosphere, as well as the freshwater flux on top of the ice. Heat transfer between the sea-ice and the atmosphere is given by $Q_{ia}\rho_i L$. Heat transfer between the ocean and the sea ice is given by $\rho_0 C_p K(T - T_f)\rho_i L$ where T is either T or T_1. Sea ice growth due to precipitation is given by the term $F\sigma$.

The set of differential Eq. (2 – 5) is solved using the ODE15s (Ordinary Differential Equation) solver incorporated in Matlab. The ODE15s solver is a variable-step, variable-order solver based on an algorithm by Klopfenstein (1971) using numerical differentiation formulas (NDFs) orders 1 to 5. Tolerances for the absolute and relative error are used to increase the accuracy of the model; these tolerances are set to 10^{-10} and 10^{-8}, respectively.

2.2 ~~Model Setup and Case Description~~CESM simulation

In this study we use the results of the CESM simulation of van Westen and Dijkstra (2020a). For a full description how the simulation was performed we refer to van Westen et al. (2020). In van Westen and Dijkstra (2020a) the high resolution version of the CESM was used with a horizontal ocean and sea ice resolution of 0.1° (10 km). The atmospheric component has a horizontal resolution of 0.5° (50 km). The ocean (atmosphere) has 42 (30) non-equidistant depth (pressure) levels. The model was run for year 2000 conditions. These conditions do not represent a climate in equilibrium but it was used since it is close to our current observations. For this study we have used model years 150-250, which were detrended as described in van Westen and Dijkstra (2020a).

2.3 Model Setup and Case Description

The original polynya model of Martinson et al. (1981) is obtained from the model formulation above by setting the horizontal advective fluxes (F_{T1}, F_{S1}, F_{T2} and F_{S2}) to zero and by setting the subsurface layer values of temperature and salinity to constant values. We consider two cases of this configuration of the model, which only differ by the value of K_S used. The higher value of K_S (case MKH: Martinson K_S high) results in more salt transfer from the subsurface layer to the surface layer (than in case MKL (Martinson K_S low) with the lower value of K_S) increasing the density of the surface layer, making it more susceptible to overturning (Table 1).

The three cases with a dynamic subsurface layer are differentiated on the inclusion of the different components of the subsurface forcing. Case PFB (Periodic Flux Both) uses both a time varying subsurface heat and salt flux. Case PFH (Periodic Flux Heat) uses a time varying subsurface heat flux and the subsurface salt flux is set to a constant value. Case PFS (Periodic Flux Salt) uses a time varying salt flux and the heat flux is set to a constant value. The aim of this configuration is to reproduce the general features of the CESM simulation of van Westen and Dijkstra (2020a), where the observed multidecadal variability of the MRP events is one of the key features. The different cases are used to assess the importance of the different components of the subsurface forcing on the MRP formation.

Parameter values for each case are displayed in Table 2. The parameter values are either taken from Martinson et al. (1981), or based on the CESM simulation of van Westen and Dijkstra (2020a), or they are determined through tuning of the model. For the CESM simulation, we determined spatial-averaged quantities over the Polynya region (2°E - 11°E $\times$ 63.5°S - 66.5°S), where an MRP forms in the CESM (van Westen and Dijkstra, 2020a). The aim of the model is to investigate multiple polynya events, and therefore it is necessary to tune the stratification. The stratification can be either too strong and no overturning occurs, or the stratification is too weak, and the water column overturns each year. To obtain multiple polynya events the heat and salt fluxes between the two layers and between the sea ice and the surface layer are tuned.

The typical depth of the layers has been determined from the CESM simulation of van Westen and Dijkstra (2020a). The depth of the surface layer (h) is set to 160 m, because the potential density shows a clear homogeneous layer below 160 m (Fig. 2a). This compares well to the value used in Kurtakoti et al. (2018) (150 m) but is smaller than the value used in Martinson et al. (1981) (200 m). The depth of the entire layer (H) is set to 2000 m. This is the approximate mixed layer depth during convective

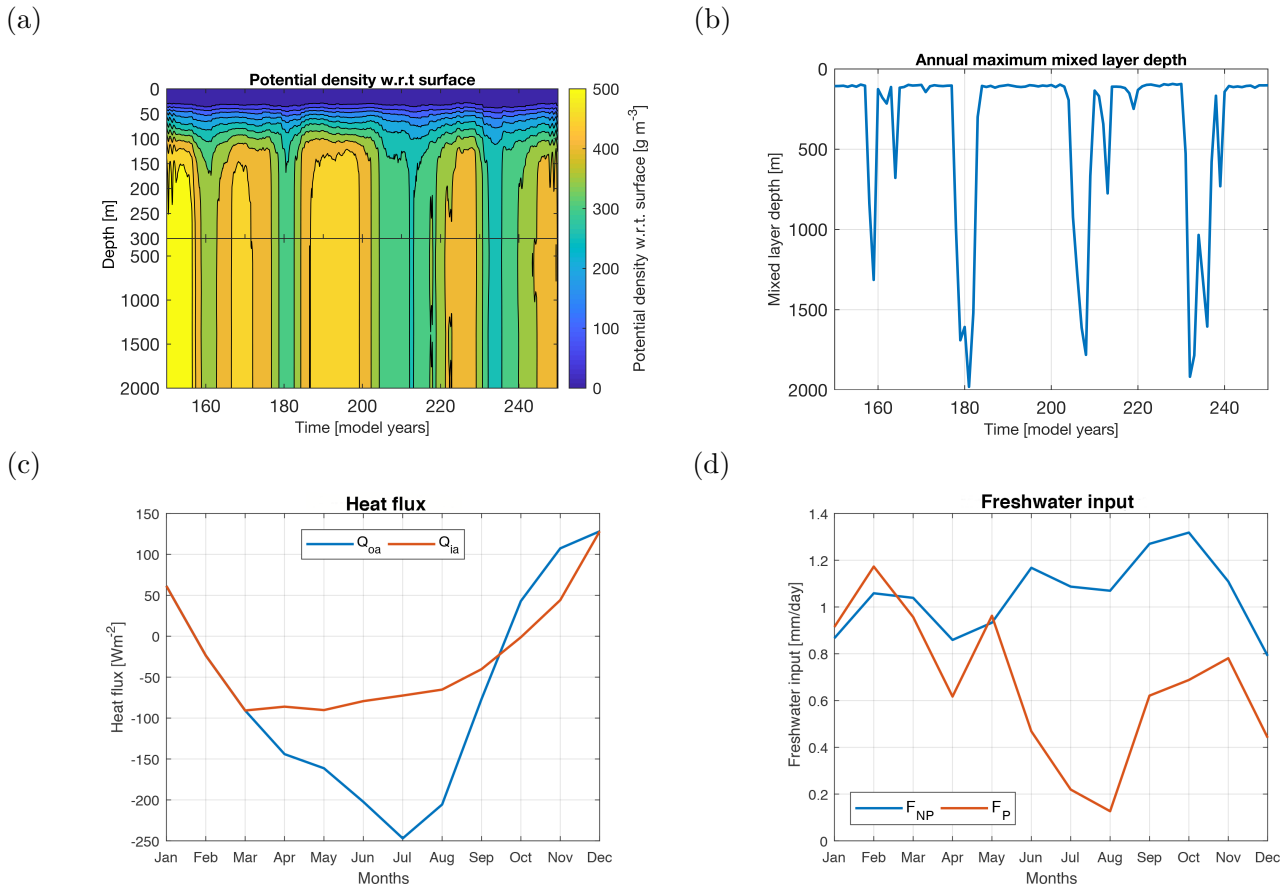

Figure 2. (a) Potential density over depth for CESM model years 150 – 250 from the CESM simulation of van Westen and Dijkstra (2020a) smoothed with a 5-year running mean. (b) The annual maximum mixed layer depth for CESM model years 150 – 250 determined from the CESM simulation of van Westen and Dijkstra (2020a). (c) The heat fluxes in W m^{-2} (see also Table 3) is determined from the CESM simulation of van Westen and Dijkstra (2020a). These values are interpolated linearly in the model as displayed in this figure. (d) The freshwater input in mm/day (see also Table 3) is determined from the CESM simulation of van Westen and Dijkstra (2020a). All quantities are spatially averaged over the Polynya region (2°E - 11°E $\times$ 63.5°S - 66.5°S).

Table 1. Overview of the different cases considered and values for the diffusivity parameters for heat (K_T) and salt (K_S) transfer between the two layers for each case. A model component can either be included ('on') or excluded ('off'). The model component 'dynamic T_2 and S_2' stands for an active subsurface layer. If this component is excluded, the set up uses a subsurface layer with constant density. If either F_{T2} or F_{S2} is excluded, the background value corresponding to the flux is set constant. The model components containing 'F' represent fluxes with subscripts representing the horizontal heat (T) and salt (S) fluxes in either the surface (1), or subsurface (2) layer.

Model Case	Dynamic T_2 and S_2	F_{T1}, F_{S1}	F_{T2}	F_{S2}	K_T [10^{-6}m s^{-1}]	K_S [10^{-6}m s^{-1}]
MKL	off	off	off	off	5.00	1.375
MKH	off	off	off	off	5.00	2.00
PFB	on	on	on	on	~~2.82~~ 3.1	~~2.82~~ 3.1
PFH	on	on	on	off	~~2.80~~ 3.1	~~2.80~~ 3.1
PFS	on	on	off	on	~~2.80~~ 3.1	~~2.80~~ 3.1

events in the CESM simulation (Fig. 2b). This magnitude corresponds well to values presented in Fahrbach et al. (2011) for the lower limit of where Weddell Sea Deep Water is found, and in Dufour et al. (2017) for the depth of the subsurface layer. It is, however, half the size of the value used in Martinson et al. (1981) ($H = 4000$ m). Cases MKL and MKH use different subsurface temperature and salinity values. These values are the time-mean temperature and salinity of the subsurface forcing (shown in Section 3.1 and as dashed lines in Fig. 3) in the PFB, PFH and PFS cases. The used values are ~~$T_2 = 0.8609$ °C and $S_2 = 34.7549$~~ $T_2 = 1.175$ °C and $S_2 = 34.7847$ g/kg, where Martinson et al. (1981) use $T_2 = 0$°C and $S_2 = 34.66$ g/kg.

The turbulent exchange coefficient K, and the exchange coefficients K_T and K_S have been used as tuning parameters for the different cases. The coefficient K is set to 1×10^{-4} ms^{-1} for all cases (in Martinson et al. (1981) this value is 3×10^{-4} ms^{-1}). The values of K_T and K_S per case are shown in Table 1. To compare the magnitude of these parameters with values used in literature the values need to be converted from ms^{-1} to m^{2}s^{-1}, which is the usual unit for vertical diffusivity parameters. This is done by multiplying these values with the depth of the surface layer (i.e. 160 m). This results in values between 2.2×10^{-4} m^{2}s^{-1} and ~~8×10^{-4} m^{2}s^{-1}~~ 5×10^{-4} m^{2}s^{-1}. Comparable values are found in a model study of Dufour et al. (2017) for this same location and in observations (Shaw and Stanton, 2014). The values used in this study are up to a factor 10 larger than the values used in Martinson et al. (1981) ($K_T = 7 \times 10^{-7}$ ms^{-1} and $K_S = 10^{-7}$ ms^{-1}).

Initial conditions of the model affect the long-term behaviour of the model. Besides, the initial regime of the model should match with initial conditions. For example, when starting in a sea-ice covered regime, the initial conditions for sea ice should be $\delta > 0$. Another important initial condition is the initial stratification. If the initial stratification is too weak, the model will overturn each year. In this specific case, it is not possible to study multidecadal variability in polynya formation. Therefore, each model simulation is initiated on January 1 with the following conditions: $T_1 = 0.1$°C, $S_1 = 34.2$ g/kg and $\delta = 1$ m.

Table 2. Standard parameter values used in the model. Superscripts show whether the parameter value is determined from the CESM simulation of van Westen and Dijkstra (2020a) (C), or determined through tuning (t), or taken from Martinson et al. (1981) (M).~~Bars~~ Overbars represent mean values (averaged over a 25 year cycle).

Parameter	Value	Parameter	Value	Parameter	Value
h^C [m]	160	ρ_i^M [kg m^{-3}]	900	C_P^M [J kg^{-1} °C^{-1}]	4.18×10^3
H^C [m]	200	α^M [°C^{-1}]	5.82×10^{-5}	L^M [J kg^{-1}]	2.5×10^5
$\overline{T_2}^C$ [°C]	0.8603	β^M [(g/kg)$^{-1}$]	8×10^{-4}	σ^M [g/kg]	30
$\overline{S_2}^C$ [g/kg]	34.7549	ρ_0^M [kg m^{-3}]	1000	T_f^M [°C]	-1.86
K^t [m s^{-1}]	10^{-4}				

3 Results

In Section 3.1 the forcing conditions of the MRP box model, as determined from the CESM simulation are discussed. ~~Section~~ A discussion on how polynyas form in the CESM is presented in Section 3.2. Section 3.3 presents an analysis of the general model behaviour, with cases MKL and MKH being discussed in Section 3.4. The results for the cases PFB, PFH, and PFS are shown in Section 3.5. In the last Section 3.6, the effects of additive noise in the freshwater flux on the model behaviour for the cases MKL and PFB are described.

3.1 Forcing Conditions

The model is forced by a monthly varying heat flux (Q_{oa} or Q_{ia}) and a monthly varying freshwater flux (F) that are repeated for each model year (Fig. 2c,d, Table 3). The monthly-averaged heat fluxes are retained from the CESM. The fluxes are spatially averaged over the polynya region (2°E – 11°E × 63.5°S – 66.5°S, black box in Fig. 4) defined in van Westen and Dijkstra (2020a). The surface heat flux strongly increases when the sea-ice fraction is lower than 0.5 in the CESM (not shown). Therefore, sea-ice fractions lower (higher) than 0.5 represent a sea-ice free (covered) regime with the ocean-atmosphere (sea ice-atmosphere) heat flux noted by Q_{oa} (Q_{ia}). Note that the MRP box model has a discrete sea-ice fraction of either 0 or 1. The monthly averaged heat fluxes are linearly interpolated in time. We do not use the sea ice-ocean flux from CESM, since this flux is already represented in the model equations (e.g. by the term $K(T - T_f)$ in equation 4).

There is a tendency of more evaporation (decrease in F) when an MRP forms. Therefore, the model uses different values for the freshwater fluxes during a polynya period (F_P) and during a non-polynya period (F_{NP}); these freshwater fluxes are also retained from the CESM simulation, and, just as the heat fluxes, spatially averaged over the polynya region in van Westen and Dijkstra (2020a). The monthly-averaged freshwater fluxes are also linearly interpolated in time. The yearly freshwater input is 0.38 m and 0.24 m for non-polynya years and polynya years, respectively. The yearly freshwater input of $F = 0.38$ m is within the range presented in Martinson et al. (1981) (0.38 – 1.73 m), this range based on limited and outdated observations. These observations do not include polynya years, and therefore they are not necessarily representative for the freshwater input during a polynya event.

Table 3. Ocean-atmosphere heat flux (Q_{oa}) in Wm^{-2}, sea ice-atmosphere heat flux (Q_{ia}) in Wm^{-2}, and the freshwater input (F=P-E) in mm/day for polynya (P) and non-polynya (NP) regimes per month determined from the CESM simulation of van Westen and Dijkstra (2020a). Positive values represent fluxes going into the ocean or the sea ice (warming and net precipitation). Negative values represent fluxes going to the atmosphere (cooling and net evaporation). All fluxes retained from the CESM simulation are spatially averaged over 2°E – 11°E × 63.5°S – 66.5°S.

Month	$Q_{oa}[\mathrm{Wm}^{-2}]$	$Q_{ia}[\mathrm{Wm}^{-2}]$	F_P[mm/day]	F_{NP}[mm/day]
Jan	61.4	61.4	0.91	0.87
Feb	-23.6	-23.6	1.17	1.06
Mar	-90.8	-90.8	0.96	1.04
Apr	-144.1	-86.1	0.62	0.86
May	-161.3	-90.3	0.96	0.93
Jun	-202.3	-79.3	0.47	1.17
Jul	-246.9	-72.5	0.22	1.09
Aug	-205.6	-65.2	0.13	1.07
Sep	-76.9	-40.3	0.62	1.27
Oct	-43.0	-1.2	0.69	1.32
Nov	107.4	44.1	0.78	1.11
Dec	128.2	128.2	0.44	0.79

Values for the four horizontal advective fluxes (F_{T1}, F_{S1}, F_{T2} and F_{S2}), background temperatures (T_{b1} and T_{b2}) and salinities (S_{b1} and S_{b2}) are obtained from the CESM simulation. The first layer uses a constant background temperature ($T_{b1} = -0.33$°C). The constant background salinity (S_{b1}) for the surface layer is slightly changed to tune the model (from 34.5 to 34.4818 g/kg). This is necessary to be able to simulate multiple polynya events. In the CESM, the background temperature and salinity of the subsurface layer (200 – 1000 m depths) are periodically varying as shown in Fig. 3. The dominant period in CESM is 25-years (not shown). This translates into a prescribed 25 year cycle for F_{T2} and F_{S2}. The time mean of T_{b2} and S_{b2} are also shown in Fig. 3.

These horizontal fluxes are used to make sure the water masses in the box do not drift away from the surrounding water masses. We have used fitted background states since we are using a highly idealized model incapable of reproducing the CESM simulation accurately. Using a fitted background makes it possible to test high level hypotheses with this model. ~~For all horizontal fluxes~~ All the horizontal fluxes are dependent on a relaxation timescale (τ)~~is used~~, which is based on the advective time scale of the Weddell Gyre ($\tau_A = L/U$). The typical velocity scale in the Weddell Gyre is on the order of 5×10^{-2} m s^{-1} (Klatt et al., 2005), and the typical length scale of the Weddell Gyre is 10^6 m. This results in an advective time scale of 230 days. To be able to represent multiple MPR events in the model, τ is chosen as (tuned to) $\frac{1}{200\ days}$.

3.2 Polynya formation in the CESM

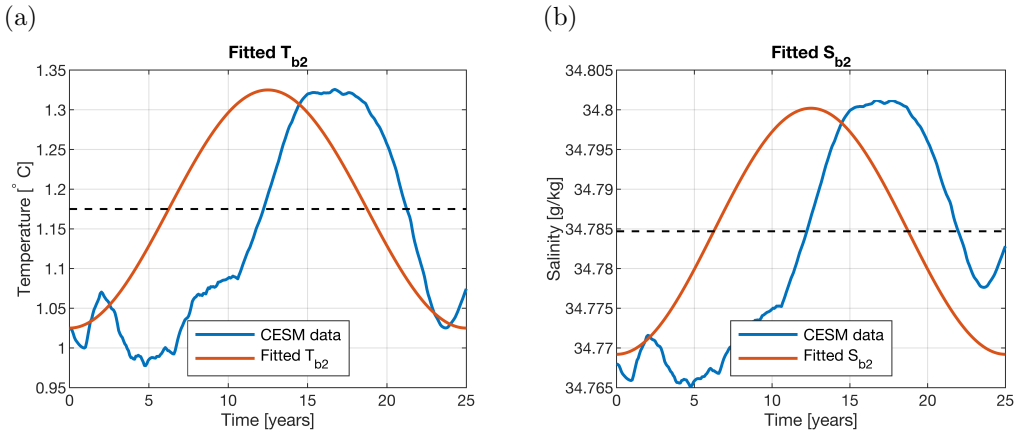

Figure 3. (a) Subsurface background temperature (T_{b2}) (red) used in the extended model set up fitted to model years ~~210-235~~ 206-231 of the CESM simulation of van Westen and Dijkstra (2020a) (blue). The CESM simulation data (blue line) is averaged over depth (200-1000m), and smoothed with a 5-year running mean. The black ~~dotted~~ dashed line represents the time mean used in MKL and MKH. (b) Same as (a) but now for the subsurface background salinity (S_{b2}). The CESM data is spatially averaged over the region of ~~2~~11°E – ~~11~~12°E × 63.5°S – 66.5°S~~.~~, which is upstream of the polynya region defined in van Westen and Dijkstra (2020a)

In this section we discuss how polynyas form in the CESM simulation of van Westen and Dijkstra (2020a). The high resolution version of the CESM has been reported to show a bias in sea ice thickness (thinner), and a smaller areal extent around Antarctica (Small et al., 2014). van Westen and Dijkstra (2020b) show in their study that their simulated August sea-ice thickness and extent falls within observational bounds as shown in an observational-model study in this part of the Weddell Sea (Holland et al., 2014) , which suggests that the bias is not present in this part of the Weddell Sea in the CESM simulation.

Polynya formation in the CESM can occur due to embayments, which means that sea ice grows around a patch of open ocean. In the CESM simulation of van Westen and Dijkstra (2020a) the Maud Rise region is first completely covered with sea ice, though the sea ice is less thick in the Maud Rise region (Fig. 4a, b). In year 231 the polynya forms in mid August (Fig. 4c), after which it extends to a larger polynya at 01-11-231 (Fig. 4d). This analysis, and the analysis in van Westen and Dijkstra (2020b) show that polynya formation in the CESM simulation is not caused by a bias in the mean state of the model but most likely due to the processes described in van Westen and Dijkstra (2020a, b), i.e. deep convection initiated in the subsurface.

3.3 Yearly Repeated Cycles

The MRP box model displays three types of yearly cycles, which are shown schematically in Fig. 5 for the surface box temperature and salinity. Note that the salinity axis has no values. If actual values would have been used, the cycles would overlap (see e.g. in Fig. 7c). In Fig. 5, each cycle starts at 'A' and follows in alphabetical order where each letter stands for a regime transition. We use the following definition for MRP formation in this box model: An MRP has formed when the sea ice has melted away completely while there is still ~~atmospheric~~ ocean cooling (negative heat flux).

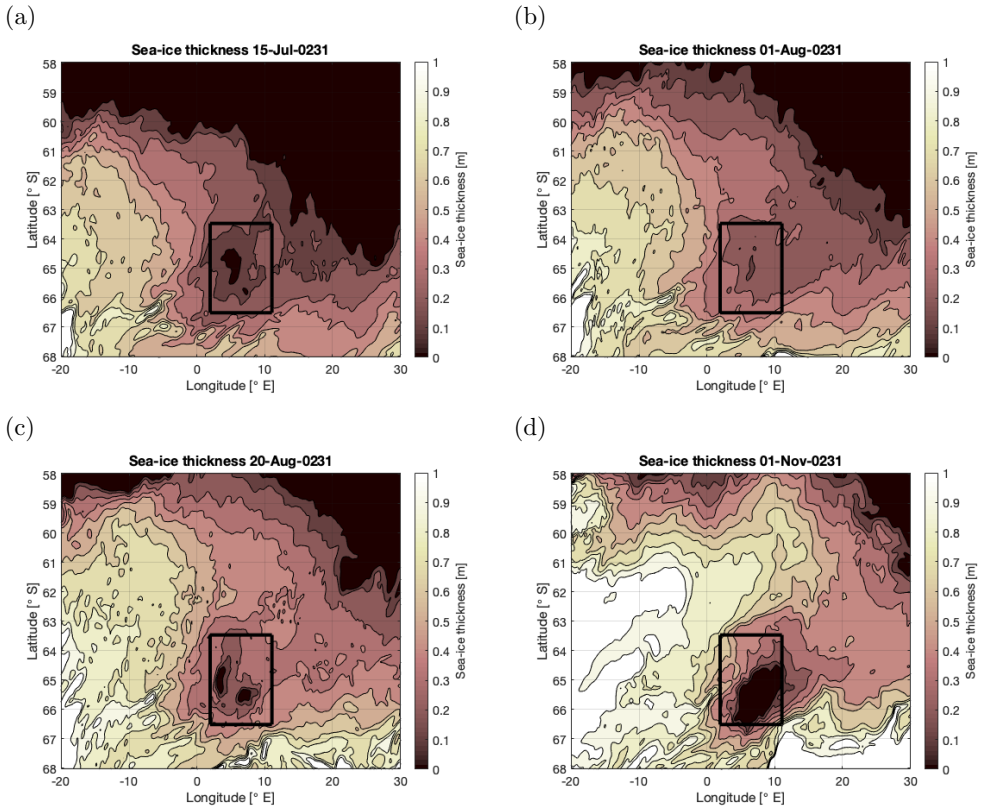

Figure 4. Sea-ice thickness for four days in a year with polynya formation in the CESM simulation of van Westen and Dijkstra (2020a). The black box represents the polynya region as defined in van Westen and Dijkstra (2020a).

For the 0-overturn cycle, the model cycles between regime II (stable, sea-ice free) and IV (stable, sea-ice covered). At 'A', the model transits from regime II $\rightarrow$ IV because the surface layer reaches the freezing temperature. During sea-ice growth, brine is rejected resulting in an increase of the surface salinity. During austral spring, the sea ice melts leading to an increase of the freshwater flux and consequently salinity levels decrease. At 'B', the model transits back to regime II since all the sea ice has melted. Next, the surface layer temperature T_1 is mainly controlled by the atmospheric heat flux, which is positive (negative) during austral summer (autumn). When the model is cooled down to freezing temperatures, the model transits in 'A' to regime IV and the (seasonal) cycle continues.

For the 1-overturn cycle, where the model overturns once, the surface layer also reaches freezing temperatures in 'A' and brine is rejected. The difference here is that the water column becomes statically unstable ($\rho_1 \geq \rho_2$) in 'B' and enters the overturning regime III (mixed, sea-ice covered) for a relatively short period (in the order of minutes) after which in transits back to regime IV in 'C'. Due to vertical mixing, relatively warm and saline subsurface water is mixed upwards and melts the sea ice; a polynya forms. During polynya formation, the model transits to regime II in 'D'. Similar to the 0-overturn cycle, the

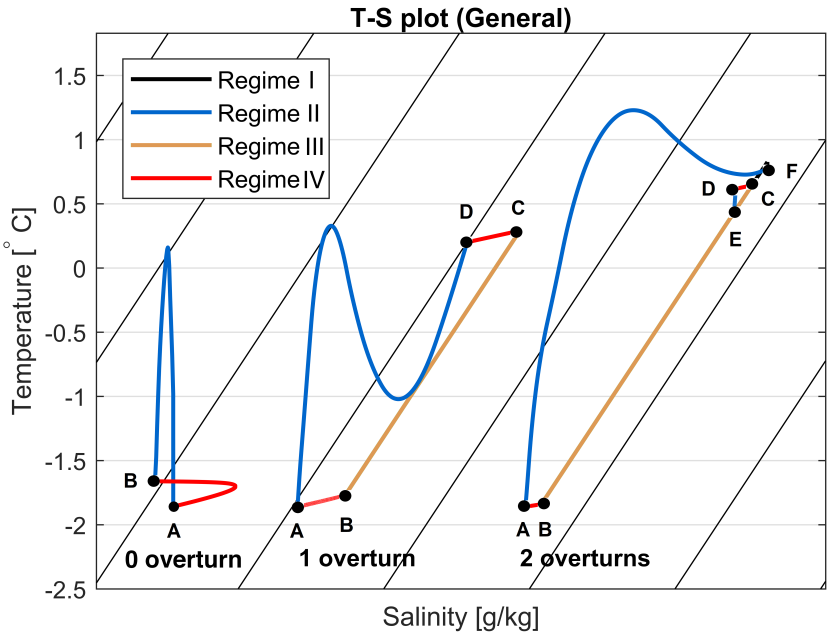

Figure 5. Schematic T_1-S_1 diagram with arbitrary scale on the salinity axis increasing to the right, showing three general cycles: 0-overturns (left), 1-overturn (middle), and 2-overturns (right) each year. The different model regimes are displayed in black (I), blue (II), orange (III), and red (IV). The letters (A-F) represent regime changes. The cycle starts at A, and follows the alphabetical order. The black contours represent isopycnals, and density increases from left to right. No values are used on the salinity axis for clarity. If values would have been used the cycles would overlap.

surface layer is controlled by the atmospheric heat flux for the remaining part of the year (austral winter – autumn). This cycle is similar to the one reported in Martinson et al. (1981).

For the 2-overturn cycle, the model transits through all four regimes. The first part of the cycle (A – D) is similar to the 1-overturn cycle and a polynya forms in 'D' but considerably less sea ice forms between 'A' and 'B' compared to the 1-overturn cycle. After 'D', the surface layer is cooled during austral winter, but the difference here is that the surface layer becomes static unstable in 'E' and switches to regime I (mixed, sea-ice free). After the model state becomes statically stable in 'F', it stays stable for the remaining part of the year.

3.4 Cases MKL and MKH

When the MRP box model was configured with parameter values and numerical schemes as reported in Martinson et al. (1981), their results could not be reproduced. Unfortunately, there is an incomplete parameter documentation in Martinson et al. (1981). In addition, it is not clear how the atmospheric heat fluxes were interpolated in time. For the cases MKL and MKH (for which

parameters are slightly different than the ones in Martinson et al. (1981)), the MRP box model is spun-up for 75 years and continued for another 25 years (model years 76 – 100).

The results for the cases MKL and MKH are shown in Fig. 6a-c and Fig. 6d-f, respectively. For both cases, the density of both layers, the sea-ice thickness and a T-S diagram are shown for the last 25 years. MKL remains in the 0-overturn cycle (Fig. 5) while in MKH (larger K_S), a 2-overturn cycle is found~~; during each year~~. In Fig. 6b and e we can see that the sea-ice thickness shows the same yearly cycle every year. For temperature and salinity in the surface layer this can be seen in Fig. 6c and f. This shows there are no variations in the model with a period larger than 1 year. In case MKH we see a little sea-ice growth each year followed by overturning and subsequent sea-ice melt. Using our definition of polynya formations, we can state that each year a polynya forms, and therefore case MKH can be considered as one long polynya period. In summary, for both cases MKL and MKH only yearly cycle solutions are found under the given forcing. Both solutions do not correspond with MRP events in observations, since no persistent MRP is found over a few years (Campbell et al., 2019).

In the CESM results of van Westen and Dijkstra (2020a), the MRP reappeared every 25 years and an MRP event lasted for about 6 consecutive years. Between model years 210 – 230, prior to MRP formation, no deep convection occurred, and the region was statically stable (van Westen and Dijkstra, 2020b); in model years 231 – 237, an MRP formed. A T-S diagram of the surface layer (upper 160 m) from the CESM results (Fig. 7) also shows that the temperature and salinity increase over time. Clearly, the MRP box model results for the cases MKL and MKH, under the CESM-derived surface forcing, cannot reproduce the CESM results as in van Westen and Dijkstra (2020a).

3.5 Cases PFB, PFH and PFS

Also, for the cases PFB, PFH and PFS, the MRP box model is spun-up for 75 years and continued for another 25 years (model years 76 – 100). In case PFB (Fig. 8) both heat and salt subsurface flux forcings are included. Based on the fitted subsurface fluxes (Fig. 3), and Eq. (1), the effects of the background subsurface temperature and salinity on the density almost compensate each other. There is a relatively small subsurface density maximum ~~(1027.7530 kgm^{-3})~~ between model years 87 – 88 (red line Fig. 8a). The cycle shown in Fig. 8 is repeated every 25 years, which means multidecadal recurring polynya events are simulated. Of the simulated 25 years, there are 7 ~~non-polynya~~ polynya years and 18 ~~polynya~~ non-polynya years. The polynyas are visible by reduced sea-ice maxima (mean of ~~0.2~~ 0.21 m for polynya years versus a mean of ~~0.32~~ 0.29 m for non-polynya years; Fig. 8b). In a 25-year cycle, the ~~first overturn after a non-polynya period occurs approximately 4 years after the subsurface heat and salt accumulation have reached their maximum. These~~ water column overturns when the subsurface density is approaching its minimum. We can also see that years with overturning can be separated by a year without overturning (e.g. in Fig. 8 in year 76 and 78 there is overturning, but not in year 77). The subsurface processes also influence the characteristics of the surface layer (Fig. 8c). In cases MKL and MKH the yearly cycles overlap each other but in the case PFB the yearly cycles are different as a response to the subsurface heat and salt accumulation which is also seen in the CESM simulation (Fig. 7).

Whereas PFB uses both subsurface fluxes (heat and salt), case PFH (Fig. 9) only uses a time-varying subsurface heat flux forcing. By thermal expansion, the subsurface density decreases and the water column becomes statically unstable in model

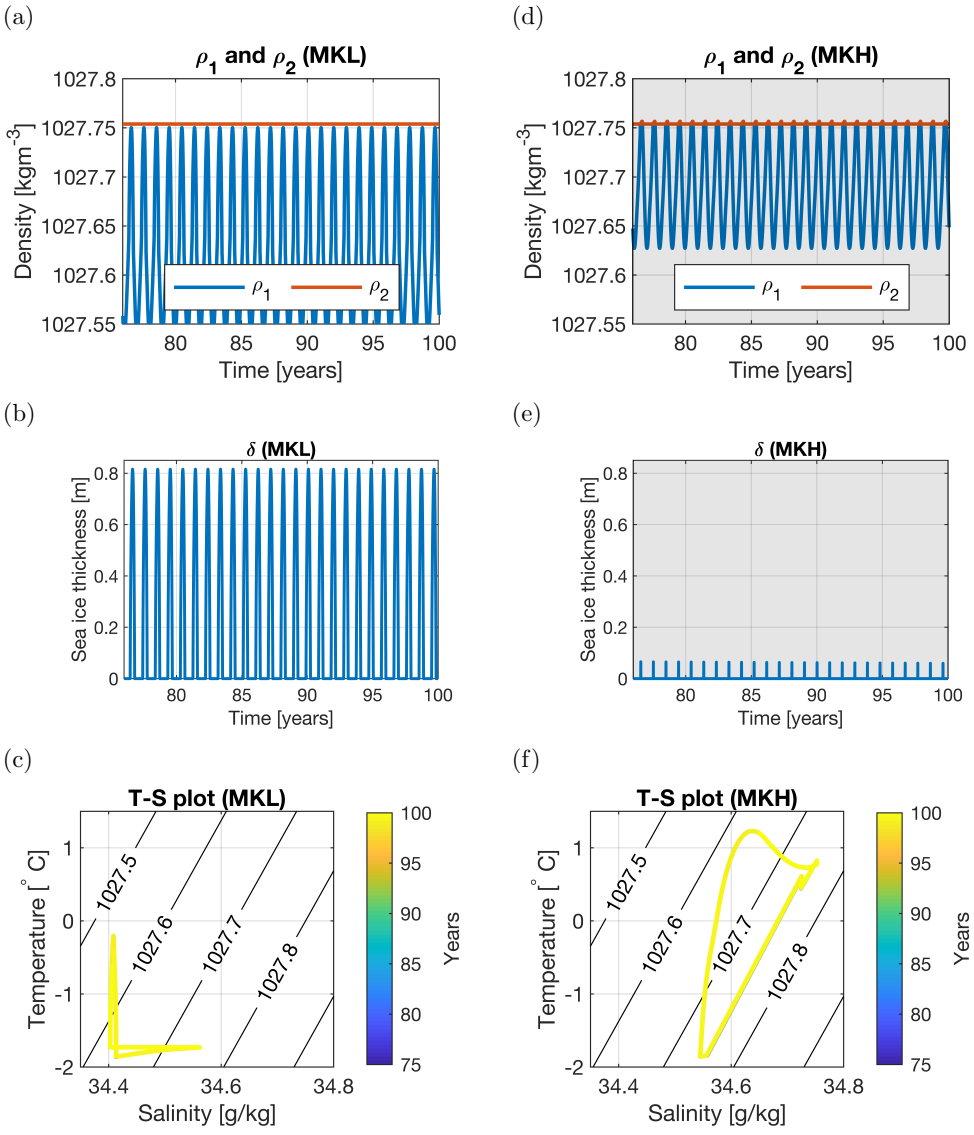

Figure 6. Years 76-100 for case MKL (a-c; $K_S = 1.375 \times 10^{-6}$ ms^{-1}) and MKH (d-f; $K_S = 2 \times 10^{-6}$ ms^{-1}) . (a, d) Density of the surface (blue) and subsurface (red) layer. (b, e) Sea-ice thickness. (c, f) T-S plot of the temperature and salinity of the surface layer. Colouring of the curves represents time, ranging from year 76 (blue) to year 100 (yellow). Only the last year is visible, because previous years have the same yearly cycle. The direction in time is the same as in Fig. 5. The black contour lines represent the density in kg m^{-3}. Shading represents polynya years.

year ~~84.~~ 86. During vertical mixing, relatively low sea-ice fractions are found compared to the stable model years. Of the simulated 25 years, there are ~~12~~13 non-polynya years and ~~13~~12 polynya years. Note that ~~the polynya years are almost the~~

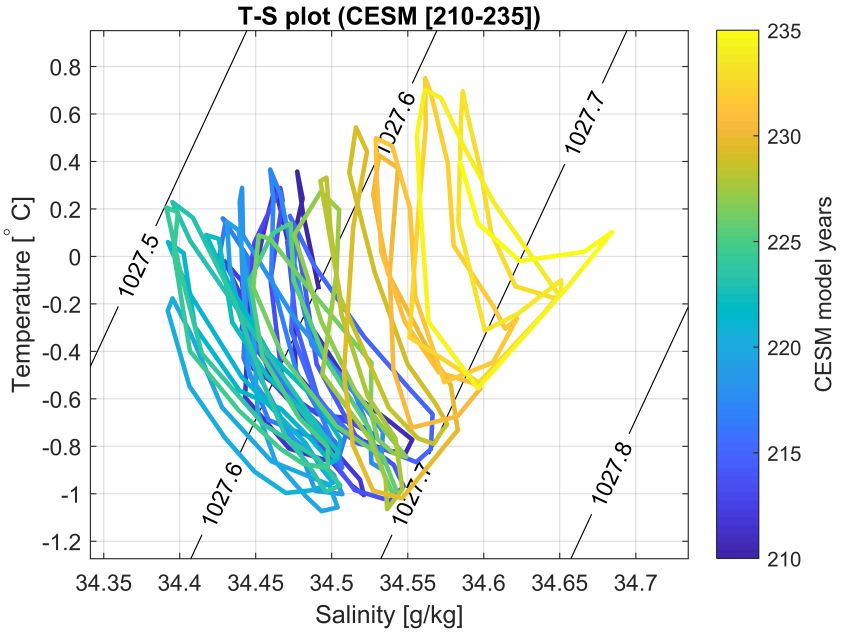

Figure 7. T-S plot of model years 210 – 235 from the CESM simulation (van Westen and Dijkstra, 2020a). The model is based on monthly values of the temperature and salinity averaged over the surface layer (0 – 160m) over the Polynya region (2°E - 11°E × 63.5°S - 66.5°S). The colour coding represents time (year 210 is blue, year 235 is yellow). The polynya period captured in this plot is between years 231 (orange) and ~~235.~~ 235 (yellow). The black contour lines represent density in kg m^{-3}, using a simple linear equation of state (Eq. (1)).

~~opposite when comparing to the~~ here we do have one long polynya period, which is different from what we see in the PFB case (Fig. 8). In case PFS (Fig. 10), only a time-varying salt subsurface flux forcing is considered. By haline contraction, the subsurface density increases and the water column is statically stable during relatively high levels of subsurface salinity. When subsurface salinity levels decrease over time, the water column becomes unstable and a polynya forms during model years 76 – ~~83 and years 95~~ 84 and years 94 – 100. Of the simulated 25 years, there are ~~11~~10 non-polynya years and ~~14~~15 polynya years.

In all three cases with subsurface forcing, the MRP box model is able to simulate the general features also seen in the CESM simulation (van Westen and Dijkstra, 2020a). These cases show a repeating 25-year cycle, which is the same period as the period of the subsurface forcing and the same period as seen in CESM. Where CESM has more non-polynya years than polynya years ~~, cases PFB and~~ case PFS have more polynya years, and case PFH has as many non-polynya years as polynya years. Case PFB, however, approaches the ratio non-polynya years versus polynya years seen in the CESM. Besides this difference, also the timing of the first overturn after a non-polynya period is different with respect to CESM. In CESM the first overturn occurs approximately 6 years after the subsurface heat and salt accumulation have reached their maximum. ~~PFB overturns 2 years earlier, and PFS 2 years~~ PFS overturns in approximately the same year, while PFB overturns 3 years later. Case PFH differs most, since it overturns ~~9~~ 8 years earlier, and even before the subsurface heat accumulation has reached

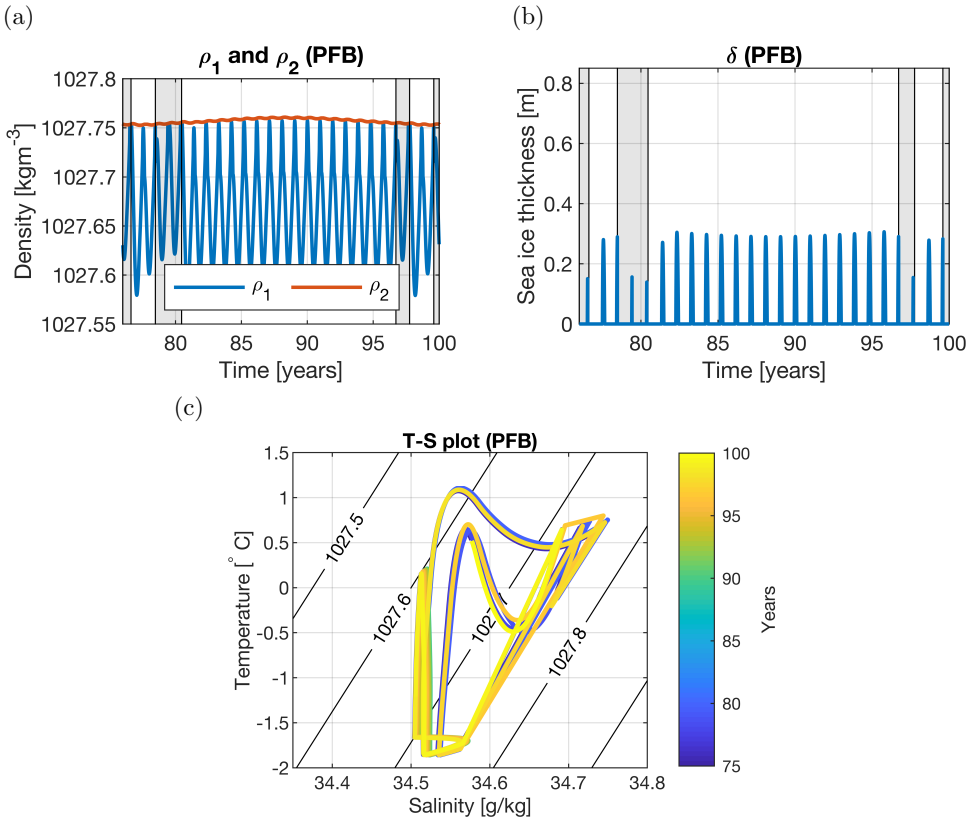

Figure 8. Years 76-100 for case PFB (both subsurface fluxes). (a) Density of the surface (blue) and subsurface (red) layer. Shading represents polynya years. (b) Sea-ice thickness. Shading represents polynya years. (c) T-S plot of the temperature and salinity of the surface layer. Colouring of the lines represents time, ranging from year 76 (blue) to year 100 (yellow). The black contour lines represent the density in kg m^{-3}. Polynyas are present between year 76 (blue), years 78-81 (blue to cyan), years 96-97 (orange), and year 99 (yellow).

its maximum. These differences are probably caused by the idealizations in the MRP box model, and most likely due to the representation of mixing in this model, compared to that in CESM.

3.6 Atmospheric Variability

In this section we analyse whether the multidecadal MRP variability, as found for the cases PFB, PFH and PFS, is robust under the influence of atmospheric variability, such as intense winter storms. This atmospheric variability is incorporated into the MRP box model by adding white noise to the surface freshwater flux. White noise was added as in Eq. (6):

$$F_N(t) = 35 \times (F(t) + \sigma_N r(t)) \tag{6}$$

where F_N is the freshwater flux with noise, F is the freshwater input without noise as in Fig. 2d, σ_N the standard deviation of the noise (0.6613 mm/day), and r is a random draw from a standard normal distribution on every time step. The ~~factor 35 g/kg~~

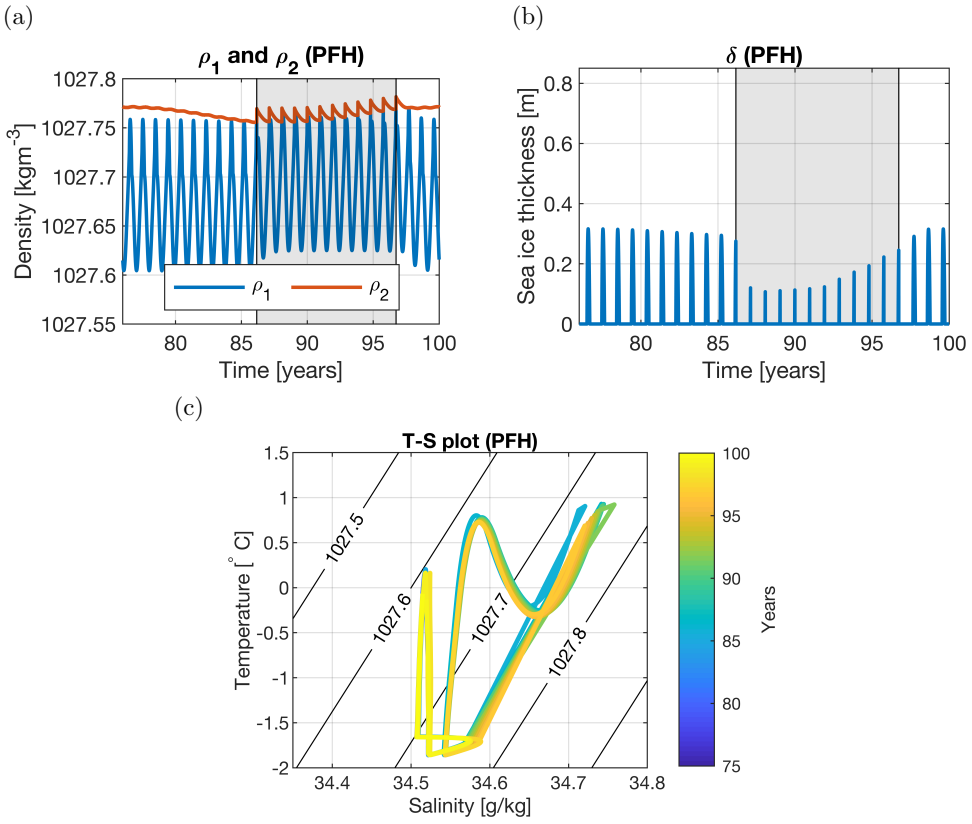

Figure 9. Years 76-100 for case PFH (with only a subsurface heat flux). (a) Density of the surface (blue) and subsurface (red) layer. Shading represents polynya years. (b) Sea-ice thickness. Shading represents polynya years. (c) T-S plot of the temperature and salinity of the surface layer. Colouring of the lines represents time, ranging from year 76 (blue) to year 100 (yellow). The black contour lines represent the density in kg m^{-3}. Polynyas are present between year 86 (cyan) and year 96 (orange).

~~is included to transform the freshwater input to a salt flux. The~~ standard deviation of the noise was determined from the CESM simulation.

Figure 11 displays the spectral power of the variables T_1 (Fig. 11a), S_1 (Fig. 11b), and δ (Fig. 11c) for case PFB. For all variables, the percentile, mean and median, the dominant period is about 25 years, the same period as the subsurface forcing and is ~~most~~ clearly visible in ~~the surface layer temperature~~ all variables (Fig. 11a). The single ensemble member also shows a dominant period of approximately 10 years, showing that the noise can also induce shorter periods of convection. Using the same white noise forcing in case MKL yields no dominant multidecadal period (not shown). As was seen in Section 3.4, the MKL case remains in 0-overturn cycle without polynyas (Fig. ~~5~~6). Atmospheric noise can cause polynyas in the MKL case. However, when MKL is forced into a polynya state, it cannot be forced out of the polynya state; a polynya forms every year. This means MKL with noise will in time show the same behaviour as MKH without noise. The combination of PFB and MKL

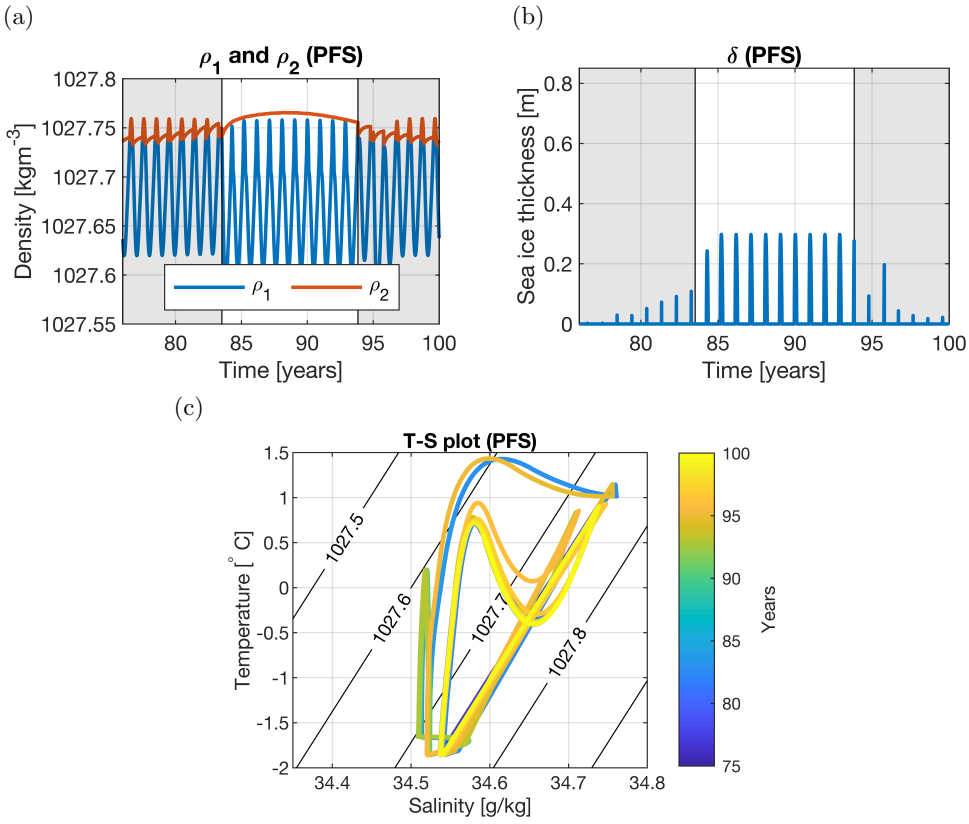

Figure 10. Years 76-100 for case PFS (with only a subsurface salt flux). (a) Density of the surface (blue) and subsurface (red) layer. Shading represents polynya years. (b) Sea-ice thickness. Shading represents polynya years. (c) T-S plot of the temperature and salinity of the surface layer. Colouring of the lines represents time, ranging from year 76 (blue) to year 100 (yellow). The black contour lines represent the density in kg m^{-3}. Polynyas are present between year 76 (blue) and 83 (cyan), and after year 94 (orange to yellow).

shows that atmospheric variability can alter the timing of polynya formation but the dominant period is set by subsurface fluxes of heat and salt.

4 Summary and discussion

In this study, an idealized box model, slightly extended from that in Martinson et al. (1981), was used to investigate the importance of surface forcing and subsurface forcing on Maud Rise Polynya (MRP) formation, in particular to understand in more detail the CESM results in van Westen and Dijkstra (2020a). The extensions made are a dynamic subsurface layer, and horizontal subsurface heat and salt fluxes to both the surface and the subsurface layer. Even though the results in Martinson et al. (1981) could not be reproduced exactly (due to incomplete information), the qualitative behaviour of the MRP box model (reduced to the case used in Martinson et al. (1981)) was the same.

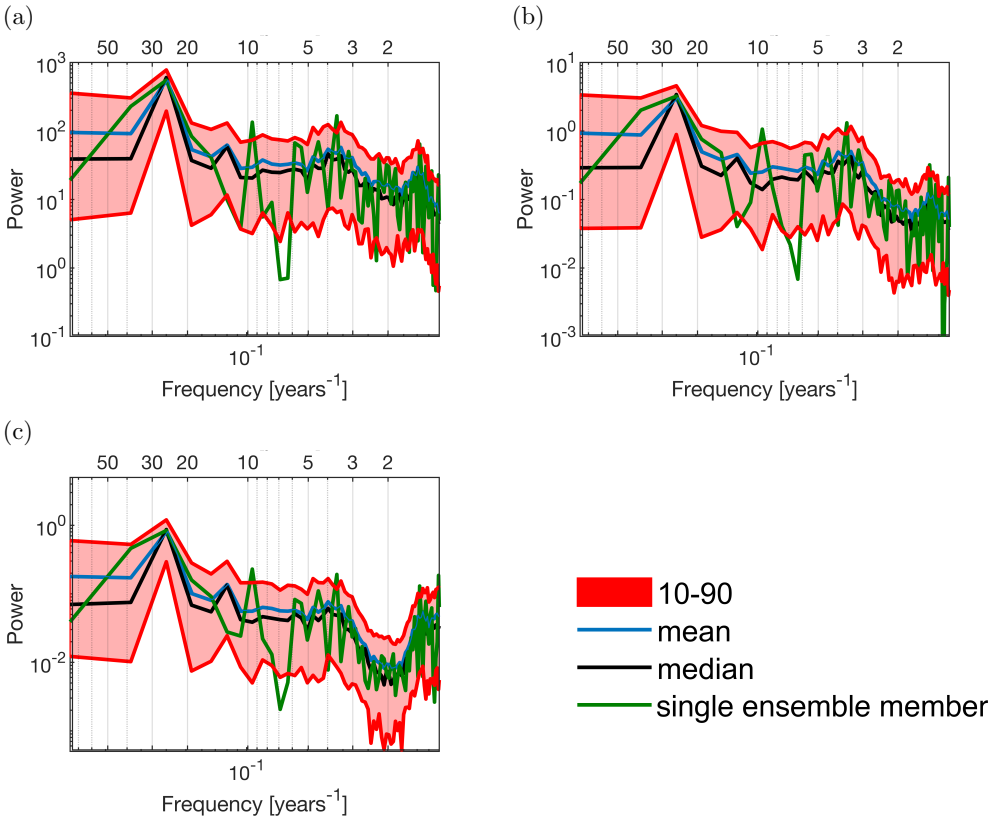

Figure 11. Spectral analysis for variables (a) T_1, (b) S_1, and (c) δ for case PFB (both subsurface fluxes). The analysis is based on 100 ensemble members. Each ensemble member contains the last 75 years of a 100 year run to exclude spin up effects. The red band represents the ensemble members between the 10$^{\text{th}}$ and 90$^{\text{th}}$ percentile. Also the mean (blue), median (black) and a single ensemble member (green) are displayed. Both axes are on log scale. The top x-axis displays the period in years, the bottom x-axis the frequency in years^{-1}.

The results for the cases MKL and MKH (close to the case in Martinson et al. (1981)) show that deep convection is caused by brine rejection in a preconditioned surface layer. Brine rejection causes a rapid increase of density in the surface layer. The results (Fig. 6d-f) clearly show that this eventually induces deep convection. However, brine rejection alone cannot explain observed multiple polynya events (e.g. the 1970s and 2017 events), since brine rejection is present in all years with sea-ice growth, and not all years show deep convection and subsequent polynya formation (Fig. 6a-c). In MKL, there is no overturn (Fig. 6a-c) and in case MKH, two overturns occur each year (Fig. 6d-f). In Martinson et al. (1981), it was also shown that in time the model state will reach a yearly repeating cycle, either in regimes II (sea-ice free, stable) and IV (sea-ice covered, stable) (0-overturn cycle), or in regimes I (sea-ice free, mixed) and II (sea-ice free, stable) (2-overturn cycle). The 0-overturning case can be explained by a too strong stratification. In case MKL, the salt transfer (governed by K_S) of the subsurface layer to the surface layer is too weak to overcome the stratification. In the second solution (two overturns each year) this salt transfer towards the surface is increased, which causes static instability in the water column with mixing as a result.

In climate models, such as CESM, the water column stabilises after deep convection when the heat and salt reservoirs are depleted. This depletion leads to stabilisation of the water column by increasing the density of the subsurface layer through heat depletion. This physical process is missing in cases MKL and MKH, and therefore the MRP box model state is not able return to a non-polynya regime. However, in Martinson et al. (1981), a solution was shown with overturns in the first years, after which a stable, non-polynya cycle appeared. These overturns in the first years are the result of the initial conditions. When the model is forced by the CESM surface forcing, either a polynya forms each year (MKH) or the model stays in a stable non-polynya state (MKL). Clearly, the cases MKL and MKH cannot capture the behaviour of the CESM as found in van Westen and Dijkstra (2020a).

In cases PFB (Fig. 8), PFH (Fig. 9) and PFS (Fig. 10), subsurface forcing derived from CESM was prescribed in the MRP box model. The results showed periodic polynya events with the same dominant period as seen in van Westen and Dijkstra (2020a) caused by the periodic subsurface forcing. The subsurface forcing preconditions both the subsurface and the surface layer, after which brine rejection is essential to induce deep convection. Note that in the CESM results of van Westen and Dijkstra (2020b), brine rejection was less important as convection was initiated at the subsurface but the box model cannot capture this. The finding of van Westen and Dijkstra (2020b) that the subsurface heat flux is more dominant than the subsurface salt flux has not been confirmed, since all cases PFB, PFH, and PFS show comparable behaviour. The subsurface heat flux, however, is expected to be dominant as it influences every quantity (T_2, ρ_2, T_1, ρ_1, δ, S_1, S_2) in the model. The subsurface salt flux only affects the density and salinity of both layers, and therefore is expected to have a much smaller influence on the results. In Kaufman et al. (2020) they also found heat build up in the ocean. They attribute this build up to reduced heat loss under sea-ice covered conditions. Ocean heat advection actually seemed to counteract the heat build up. In our model such a situation does not occur, since T_2 is always larger than T_{b2} because the subsurface layer is losing heat to the surface layer. Therefore we are not able to test this hypothesis with this model.

The MRP box model is able to capture the general features of MRP formation as seen in van Westen and Dijkstra (2020a) and shows the importance of the subsurface forcing. However, the model is still too idealised to accurately capture the precise MRP formation processes in the CESM simulation. The asymmetry in the non-polynya regime versus the polynya regime was poorly captured ~~.~~is cases PFH and PFS. The asymmetry in case PFB compared best to the CESM but still showed relatively more polynya years compared to the CESM simulation. This is probably due to the difference in how vertical mixing is represented. In the MRP box model the layers are either in a stably stratified configuration with a constant layer depth, or they are completely mixed. In van Westen and Dijkstra (2020a), a KPP boundary mixed layer scheme is used. Representing the growth of the mixed layer more accurately would improve the model, and possibly would lead to a better representation of the asymmetry between the two regimes. When the mixed layer is allowed to grow more gradually, a lag is introduced in the system. This will delay the formation of a polynya. Due to this instant mixing, both temperature and salinity in the surface layer increase instantly. This results in large differences after overturning between the MRP box model results and the CESM simulation results (van Westen and Dijkstra, 2020a).

Martinson et al. (1981) were among the first to investigate the processes responsible for polynya formation. Using their model they suggested that surface processes are responsible for polynya formation, a view that is still widely supported

nowadays. What we have shown is that their model is not capable of simulating multiple polynya events as seen in observations (e.g. the 1970s, 1980, 1994, and the 2016-2017 events). When the model is extended, with most prominently periodic subsurface heat and salt accumulation, the model is capable of simulating multiple events. This can be viewed as an improvement of the original model. Furthermore, the highly idealized model is capable of qualitatively reproducing the CESM simulation of van Westen and Dijkstra (2020a). This suggests that the most important physical processes are included in the model. Our study suggests that surface related processes cannot completely explain formation nor its periodicity, if such a multidecadal period exists in the Southern Ocean. Therefore we believe that subsurface related processes need to be investigated in future research of the MRP.

Code and data availability. The model code and input files of the conceptual box model are available via GitHub: https://github.com/dboot0016/MRP_Conceptual_box_model. CESM model data are available upon request from the authors

Appendix A: Regime transitions

In this appendix the conditions of the regime transitions are shown. A regime transition changes the initial conditions for the new regime. The new initial conditions are indicated with a prime. Horizontal bars above a variable represent averaging over the water column due to overturning: $\bar{X} = (hX_1 + (H-h)X_2)/H$, where X is either T or S.

$$\text{regime I} \rightarrow \text{regime II when } -\alpha\frac{dT}{dt} + \beta\frac{dS}{dt} < 0;$$
$$T_1' = T,\ S_1' = S,\ \delta' = 0,\ T_2' = T,\ S_2' = S;$$
$$\text{regime I} \rightarrow \text{regime III when } T = T_f;$$
$$T' = T_f,\ S' = S,\ \delta' = 0;$$
$$\text{regime II} \rightarrow \text{regime I when } \rho_1 = \rho_2;$$
$$T' = \bar{T},\ S' = \bar{S},\ \delta' = 0;$$
$$\text{regime II} \rightarrow \text{regime IV when } T_1 = T_f;$$
$$T_1' = T_1,\ S_1' = S_1,\ \delta' = 0,\ T_2' = T_2,\ S_2' = S_2;$$
$$\text{regime III} \rightarrow \text{regime I when } \delta = 0;$$
$$T' = T,\ S' = S,\ \delta' = 0;$$
$$\text{regime III} \rightarrow \text{regime IV when } -\alpha\frac{dT}{dt} + \beta\frac{dS}{dt} < 0;$$
$$T_1' = T,\ S_1' = S,\ \delta' = \delta,\ T_2' = T,\ S_2' = S;$$
$$\text{regime IV} \rightarrow \text{regime II when } \delta = 0;$$
$$T_1' = T_1,\ S_1' = S_1,\ \delta' = 0,\ T_2' = T_2,\ S_2' = S_2;$$
$$\text{regime IV} \rightarrow \text{regime III when } \rho_1 = \rho_2;$$
$$T' = \bar{T},\ S' = \bar{S},\ \delta' = \delta;$$

Author contributions. D.B. developed the model code, performed the numerical experiments, and analyzed the data. D.B. wrote the manuscript with input from all authors. R.M.W. and H.A.D. conceived the idea of the study and were in charge of overall direction and planning.

Competing interests. The authors declare that they have no conflict of interest.

Acknowledgements. The authors thank Michael Kliphuis (IMAU, UU) who performed the CESM simulations. The computations were done on the Cartesius at SURFsara in Amsterdam. Use of the Cartesius computing facilities was sponsored by the Netherlands Organization for Scientific Research (NWO) under the project 15556.

References

Alverson, K. and Owens, W. B.: Topographic Preconditioning of Open-Ocean Deep Convection, J. Phys. Oceanogr., 26, 2196–2213, doi:10.1175/1520-0485(1996)026<2196:TPOOOD>2.0.CO;2, 1996.

Campbell, E., Wilson, E., and Moore, G.: Antarctic offshore polynyas linked to Southern Hemisphere climate anomalies, Nature, 570, 319–325, doi:10.1038/s41586-019-1294-0, 10.1038/s41586-019-1294-0, 2019.

Carsey, F. D.: Microwave Observations of the Weddell Polynya, Mon. Weather Rev., 108, 2032–2044, doi:10.1175/1520-0493(1980)108<2032:MOOTWP>2.0.CO;2, 1980.

Cheon, W. G. and Gordon, A. L.: Open-ocean polynyas and deep convection in the Southern Ocean, Sci. Rep.-UK, 9, doi:10.1038/s41598-019-43466-2, 10.1038/s41598-019-43466-2, 2019.

Dufour, C. O., Morrison, A. K., Griffies, S. M., Frenger, I., Zanowski, H., and and co-authors: Preconditioning of the Weddell Sea polynya by the ocean mesoscale and dense water overflows, J. Climate, 30, 7719–7737, doi:10.1175/JCLI-D-16-0586.1, 10.1175/JCLI-D-16-0586.1, 2017.

Fahrbach, E., Hoppema, M., Rohardt, G., Boebel, O., Klatt, O., and and co-authors: Warming of deep and abyssal water masses along the Greenwich meridian on decadal time scales: The Weddell gyre as a heat buffer, Deep-Sea Res. Pt. II, 58, 2509–2523, doi:10.1016/j.dsr2.2011.06.007, 10.1016/j.dsr2.2011.06.007, 2011.

Francis, D., Eayrs, C., Cuesta, J., and Holland, D.: Polar cyclones at the origin of the reoccurrence of the Maud Rise Polynya in austral winter 2017, J. Geophys. Res., 0, doi:10.1029/2019JD030618, 2019.

Gordon, A. L.: Deep Antarctic Convection West of Maud Rise, J. Phys. Oceanogr., 8, 600–612, doi:10.1175/1520-0485(1978)008<0600:DACWOM>2.0.CO;2, 10.1175/1520-0485(1978)008<0600:DACWOM>2.0.CO;2, 1978.

Gordon, A. L., Viscbeck, M., and Comiso, J. C.: A Possible Link between the Weddell Polynya and the Southern Annular Mode, J. Climate, 20, 2258–2571, doi:10.1175/JCLI4046.1, 10.1175/JCLI4046.1, 2007.

Holland, D. M.: Explaining the Weddell Polynya - a Large Ocean Eddy Shed at Maud Rise, Science, 292, 1697–1700, doi:10.1126/science.1059322, 10.1126/science.1059322, 2001.

Holland, P. R., N, B., C, E., M, L., T, K. N., and R, K.: Modeled trends in Antarctic sea ice thickness, J. Climate, 27, 3784–3801, doi:https://doi.org/10.1175/JCLI-D-13-00301.1, https://doi.org/10.1175/JCLI-D-13-00301.1, 2014.

Jena, B., Ravichandran, M., and Turner, J.: Recent Reoccurrence of Large Open-Ocean Polynya on the Maud Rise Seamount, Geophys. Res. Lett., 46, 4320–4329, doi:10.1029/2018GL081482, 2019.

Jüling, A., Viebahn, J. P., Drijfhout, S. S., and Dijkstra, H. A.: Energetics of the Southern Ocean Mode, J. Geophys. Res., 123, 9283–9304, doi:10.1029/2018JC014191, 2018.

Kaufman, Z. S., Feldl, N., Weijer, W., and Veneziani, M.: Causal Interactions between Southern Ocean Polynyas and High-Latitude Atmosphere Ocean Variability, J. Climate, 33, 4891–4905, doi:https://doi.org/10.1175/JCLI-D-19-0525.1, https://doi.org/10.1175/JCLI-D-19-0525.1, 2020.

Klatt, O., Fahrbach, E., Hoppema, M., and Rohardt, G.: The transport of the Weddell Gyre across the Prime Meridian, Deep-Sea Res. Pt. II, 52, 513–528, doi:https://doi.org/10.1016/j.dsr2.2004.12.015, 2005.

Klopfenstein, R. W.: Numerical differentiation formulas for stiff systems of ordinary differential equations, RCA Rev., 32, 447–462, 1971.

Kurtakoti, P., Veneziani, M., Stössel, A., and Weijer, W.: Preconditioning and Formation of Maud Rise Polynyas in a High-Resolution Earth System Model, J. Climate, 31, 9659–9678, doi:10.1175/JCLI-D-18-0392.1, 10.1175/JCLI-D-18-0392.1, 2018.

Latif, M., Martin, T., Reintges, A., and Park, W.: Southern Ocean Decadal Variability and Predictability, Curr. Clim. Change Rep., 3, 163–173, doi:10.1007/s40641-017-0068-8, 10.1007/s40641-017-0068-8, 2017.

Le Bars, D., Viebahn, J. P., and Dijkstra, H. A.: A Southern Ocean mode of multidecadal variability, Geophys. Res. Lett., 43, 2102–2110, doi:10.1002/2016GL068177, 10.1002/2016GL068177, 2016.

Lindsay, R. W., Holland, D. M., and Woodgate, A.: Halo of low ice concentration observed over the Maud Rise seamount, Geophys. Res. Lett., 3, 1–4, doi:10.1029/2004GL019831, 10.1029/2004GL019831, 2004.

Martin, T., Park, W., and Latif, M.: Multi-centennial variability controlled by Southern Ocean convection in the Kiel Climate Model, Clim. Dynam., 40, 2005–2022, doi:10.1007//s00382-012-1586-7, 10.1007//s00382-012-1586-7, 2013.

Martinson, D. G., Killworth, P. D., and Gordon, A. L.: A Convective Model for the Weddell Polynya, J. Phys. Oceanogr., 11, 466–488, doi:10.1175/1520-0485(1981)011<0466:ACMFTW>2.0.CO;2, 10.1175/1520-0485(1981)0113C0466:ACMFTW3E2.0.CO;2, 1981.

Parkinson, C. L.: On the Development and Cause of the Weddell Polynya in a Sea Ice Simulation, J. Phys. Oceanogr., 13, 501–511, doi:10.1175/1520-0485(1983)013<0501:OTDACO>2.0.CO;2, 1983.

Reintges, A., Martin, T., Latif, M., and Park, W.: Physical controls of Southern Ocean deep-convection variability in CMIP5 models and the Kiel Climate Model, Geophys. Res. Lett., 44, 6951–6958, doi:10.1002/2017GL074087, 10.1002/2017GL074087, 2017.

Shaw, W. J. and Stanton, T. P.: Dynamic and Double-Diffusive Instabilities in a Weak Pycnocline. Part I: Observations of Heat Flux and Diffusivity in the Vicinity of Maud Rise, Weddell Sea, J. Phys. Oceanogr., 44, 1973–1991, doi:10.1175/JPO-D-13-042.1, 10.1175/JPO-D-13-042.1, 2014.

Small, R. J., Bacmeister, J., Bailey, D., Baker, A., Bishop, S., Bryan, F., Caron, J., Dennis, J., Gent, P., Hsu, H.-m., Jochum, M., Lawrence, D., Muñoz, E., diNezio, P., Scheitlin, T., Tomas, R., Tribbia, J., Tseng, Y.-h., and Vertenstein, M.: A new synoptic scale resolving global climate simulation using the Community Earth System Model, J. Adv. Model, 6, 1065–1094, doi:10.1002/2014MS000363, 10.1002/2014MS000363, 2014.

van Westen, R. M. and Dijkstra, H. A.: Southern Ocean origin of multidecadal variability in the North Brazil Current, Geophys. Res. Lett., 44, 10 541–10 548, doi:10.1002/2017GL074815, 10.1002/2017GL074815, 2017.

van Westen, R. M. and Dijkstra, H. A.: Multidecadal Preconditioning of the Maud Rise Polynya Region, Ocean Sci. Discuss., doi:https://doi.org/10.5194/os-2020-25, 2020a.

van Westen, R. M. and Dijkstra, H. A.: Subsurface Initiation of Deep Convection near Maud Rise, Ocean Sci. Discuss., 2020b.

van Westen, R. M., Dijkstra, H. A., van der Boog, C. G., A, K. C., James, R. K., and and co-authors: Ocean model resolution dependence of Caribbean sea-level projections, Sci. Rep., 10, 14 599–14 610, doi:10.1038/s41598-020-71563-0, 10.1038/s41598-020-71563-0, 2020.

Weijer, W., Veneziani, M., Stössel, A., Hecht, M. W., Jeffery, N., and and co-authors: Local atmospheric response to an open-ocean polynya in a high-resolution climate model, J. Climate, 30, 1629–1641, doi:10.1175/JCLI-D-16-0120.1, 10.1175/JCLI-D-16-0120.1, 2017.

Zanowski, H., Hallberg, R., and Sarmiento, J. L.: Abyssal Ocean Warming and Salinification after Weddell Polynyas in the GFDL CM2G Coupled Climate Model, J. Phys. Oceanogr., 45, 2755–2772, doi:10.1175/JPO-D-15-0109.1, 10.1175/JPO-D-15-0109.1, 2015.